Production of hydrogen and valuable fuels from polyethylene terephthalate waste dissolved in phenol reforming and cracking reactions via Ni-Co/CeO_2 nano-catalyst

Walid Nabgan[a], Bahador Nabgan[a], Tuan Amran Tuan Abdullah[a*], Aishah Abdul Jalil[a], Anwar Ul-Hamid[b], Muhammad Ikram[c], Abu Hassan Nordin[a], Alberto Coelho[d]

[a] School of Chemical and Energy Engineering, Faculty of Engineering, Universiti Teknologi Malaysia, 81310 Skudai, Johor, Malaysia
[b] Center for Engineering Research, Research Institute, King Fahd University of Petroleum & Minerals, Dhahran, 31261, Saudi Arabia
[c] Solar Cell Applications Research Lab, Department of Physics, Government College University Lahore, 54000, Punjab, Pakistan.
[d] Instituto de Cerámica, Departamento de Química Orgánica, Facultad de Farmacia, Universidade de Santiago de Compostela, 15782 Santiago de Compostela, Spain.

**Corresponding Author: tamran@cheme.utm.my

ABSTRACT

This research investigates the preparation of Ni-Co/CeO_2 catalysts based on impregnation and hydrothermal treatment methods for the hydrogen and valuable fuels generation from the steam reforming and cracking reactions of polyethylene terephthalate (PET) waste liquefied in phenol. PET plastic waste is environmentally harmful, mostly when it eliminated by burning or landfilling. Therefore, in this study, this waste has been dissolved in phenol for hydrogen and liquid fuel generation via catalytic steam reforming and cracking reactions. Complementary characterization techniques such as XRD, BET, FTIR, SEM, TEM, EDX, H_2-TPR, CO_2-TPD, NH_3-TPD, ICP, CHNS and TGA were used to correlate surface structure and functionality to catalytic performance of the catalysts. The hydrothermal route leads to higher catalyst activity and stability against a by-product formation such as coke, which approved by time on stream process, TGA and CHNS analysis. For an instant, at 700 ^oC of the catalytic reaction, impregnation method cause to achieve 72.8% of phenol conversion and 56% of hydrogen yield, while these factors increased when conducting the hydrothermal treatment to 83.8% and 76%, respectively. Analysis of liquid products obtained from GCMS illustrated that valuable components such as dibenzofuran, 2-methyl phenol and benzene were produced from PET cracking and phenol steam reforming reactions. This phenomenon is a vital idea to solve plastic waste recycling issues.

Keyword: synthesis, Ni-Co/CeO_2 nanosized, plastic waste, phenol, fuel

Abbreviation

D_p: Pore volume

BET: Brunauer–Emmett–Teller

CHNS: Carbon, hydrogen, nitrogen and sulphur

CO_2-TPD: Temperature-programmed desorption of carbon dioxide

CoO: Cobalt (II) oxide

E_a: Activation Energy

EDX: Energy Dispersive X-Ray

FTIR: Fourier-transformed Infrared Spectroscopy

GC-FID : Gas chromatography with flame-ionization detection

GCMS: Gas chromatography–mass spectrometry

GC-TCD : Gas chromatography with thermal conductivity detector

H_2-TPR: Temperature-programmed reduction of hydrogen

HPLC: High-performance liquid chromatography

ICP: Inductively coupled plasma

JCPDS: Joint committee on powder diffraction standards

KBr: Potassium bromide

NaOH: Sodium hydroxide

NC-Ce-hyd: Nickel-cobalt supported on cerium (IV) oxide catalyst prepared by hydrothermal method

NC-Ce-imp: Nickel-cobalt supported on cerium (IV) oxide catalyst prepared by impregnation method

NH_3-TPD: Temperature programmed desorption of ammonia

Ni-Co/CeO_2 : Nickel-cobalt supported on cerium (IV) oxide catalyst

NiO: Nickel (II) oxide

PET: Polyethylene terephthalate

r_{Ph} : Reaction rate

S_{BET}: BET surface area

SEM: Scanning electron microscope

TEM: Transmission electron microscope

TGA: Thermogravimetric analysis

V_p: Pore volume

WL: Weight loss

XRD: X-ray powder diffraction

1 Introduction

Greenhouse gas emissions and pollution are increasing, driven mainly by economic and population growth in recent years, which results in climate change and global warming. In addition to gaseous emissions, tons of solid wastes such as plastic wastes are also discarded to the environment. Countries have also challenged running out of fossil fuels and sooner or later will eventually look for alternative clean energy sources to replace fossil fuels. To solve these severe environmental threats, the liquification of plastic wastes in a dissolving agent for hydrogen production could be a great idea for sustainable and clean energy production and as well as plastic waste recycling concerns.

Phenolic compounds exist in a liquid form, and it releases from polluted industrial wastewater, agricultural and home activities and cause environmental infections. A number of methods have been implemented to eliminate phenolic materials from water, such as photocatalytic degradation, redox reactions, electrochemical oxidation, and membrane separation which are highly expensive processes. The phenolic compounds fraction in bio-oil is about 38 wt.% which considered as unwanted components [42]. Phenolic compounds are difficult to modify, can cause corrosion in pipes and combustion engines. This issue will result in increased phenol-rich tar values all around the world [48] which then negatively affect the environment and decline the value added organic carbon.

Much attention has been given to plastic waste management that still stores a large amount of energy [24, 59]. Moreover, the hydrogen component level in plastic waste is high and might enhance the chemical selectivity during its co-pyrolysis with biomass [8]. Research in this area is highly significant because various obstacles have taken on the plastic

and other forms of wastes. As the primary packaging material, plastics cause pollution to the environment that cannot be ignored, mostly when they are discarded after use, investigations in this area are of eternal significance [14]. Polyethylene terephthalate (PET) has been widely used in industrial scales such as packaging material and containers for drinking water. The lifetime of PET is very long, difficult to decompose naturally, comprises about 63 wt % of the overall plastic wastes [36] and are ideally suited for recycling. Thus, in the minimum pioneering functioning of PET waste can be critical support to the ecosystem, and this is one of the principal highlights of this research.

Catalyst plays a critical role in the PET-phenol cracking and steam reforming reactions. Several active metals such as Co, Fe, Ni, Rh, Ru, CaO, Pt, Pd have been used in the steam reforming reaction of phenol. Among them, Ni has low cost and the high ability for C-H and C-C bonds cracking [65] and causes to increase the reaction rate [11] during the steam reforming reaction. However, Ni catalyst is prone to deactivation by coke deposition on its surface due to its sintering and severe coking, which restricts their wide applications. To solve this problem, introducing another metal to the Ni could be a key factor in preventing coking phenomena. We have been stated that Co metal can break the integrity of the surface nickel ensembles which cause to nickel particle size reduction and decrease the carbon formation accordingly. We also found that bimetallic Ni-Co catalyst with higher Ni content had a superior catalytic activity in the phenol steam reforming reaction [43]. The choice of support for non-noble metal catalysts is vital to assurance long-term use. Several metal oxides such as γ-Al_2O_3 [7, 42, 53], La_2O_3 [7, 12, 17, 32], ZrO_2 [12, 32, 50, 51, 53], MgO [49-51], and CeO_2 [12, 32, 49-51, 53] has been applied for phenol steam reforming reaction for higher process efficiency. The high ionic conductivity and oxygen capability of CeO_2 materials are the reasons for being striking oxygen storing elements [13]. Utilizing of CeO_2 has been a

consequence of its amazing structural and chemical properties, which improve the active metal distribution, to increase the catalyst stability, and to modify the metal-support interaction [23].

Previous research has proved that CeO_2 has properties such as strong metal-support interaction (SMSI), and this causes to stabilize metal particles against thermal sintering [10]. Other studies have reported that supports such as CeO_2 for Ni catalysts can increase the activity of the catalyst and reduction the coke growth by enhancement of Ni dispersion on CeO_2 [26, 27]. However, the instability and easy gathering properties of nanostructured catalysts could cause the centre loss of catalytic activity, surface energy reduction and deactivation [29, 66]. Therefore it is noteworthy to study the catalyst preparation effect on the chemical and physical properties of CeO_2 support.

To our knowledge, rare studies were focused on CeO_2 nanoparticles preparation in bimetallic nickel-cobalt catalysts for the steam reforming and cracking reactions of PET-phenol. Besides, CeO_2 support with diverse morphology could display improved oxygen mobility and various strength of metal-support interaction, which may affect the gasification of deposing coke materials. Therefore, factors such as PET plastic waste recycling, hydrogen production from renewable sources, and low-cost catalyst could be critical features for environmental and economic impacts in the technology of hydrogen and valuable liquid fuel production. This research article aimed to investigate the effect of synthesis techniques of bimetallic nickel-cobalt supported on CeO_2 nanostructured catalysts on the chemical and physical properties of catalysts as well as on hydrogen and value-added fuels generation from the steam reforming and cracking reactions of PET-phenol. Catalysts were synthesized by hydrothermal, and impregnation methods and characterized via ICP, BET, XRD, EDX, SEM,

TEM, H_2-TPR, CO_2-TPD and used samples were characterized by TGA, CHNS and ICP tests. The effect of catalyst preparation on catalytic activity, stability and kinetic study, reaction rate and activation energy for PET-phenol cracking and steam reforming reactions was also examined.

2 Experimental

2.1 Preparation of Ni-Co/CeO_2 nanosized catalysts

The CeO_2 nanosized support was prepared through a hydrothermal treatment technique. Firstly, a specific amount of CeO_2 was diluted with 250 mL of deionized water with a ratio of 1:10 and mixed for two hours. Formerly 5M NaOH was included to the mixture at room temperature and mixed for an hour. The aqueous solution was then transferred to an autoclave reactor and heated at 130 ^oC for two days. The produced white liquid was then cleaned, washed and dried. The 10 wt% of Ni and Co metals with the ratio of 3:2 was then impregnated to the CeO_2 nanosized support assigned as NC-Ce-hyd. The conventional impregnation method of catalyst preparation was obtained following our earlier studies [39, 40, 43];—briefly, 90 wt.% CeO_2 and 10 wt.% Ni and Co with the ration of 3:2 were mixed in deionized water. Equation 1 was used to calculate the amount of Ni and Co from $Ni(NO_3)_2{\cdot}6H_2O$ or $Co(NO_3)_2{\cdot}6H_2O$ materials. The solution was then stirred using a magnetic stirrer at 90 °C to produce a slurry. The slurry was dry at 110 °C for 24 h and followed by calcination at 800 °C for three hours.

$$Amount\ of\ X\ (g) = 0.6\ g\ Ni(or)\ 0.4Co\ \times \frac{1\ mol\ Ni(or)Co}{58.7g} \times \frac{1mol\ X}{1\ mol\ Ni(or)Co} \times \frac{291\ g\ X}{1\ mol\ X} \quad (1)$$

2.2 Characterization of the catalysts

The crystal structure of the synthesized catalyst was detected by XRD using a Bruker D8 Advance diffractometer (Cu Kα radiation, λ = 1.5406 Å). The morphological characterization of the catalysts was made in an emission scanning electron microscope (SEM) (JEOL, JSM-6390) and in a transmission electron microscope (TEM) (JEM-2100). Elemental compositions were determined by energy-dispersive X-ray spectroscopy (EDS) analysis employing an Oxford Xmax 50 mm machine. The BET surface areas and pore size distributions of the samples were analyzed using a Beckman Coulter SA3100^{TM} instrument. Fourier-transformed Infrared Spectroscopy (FTIR) analysis was conducted on an IR-Prestige-21 Shimadzu spectrometer using pure KBr as a reference background to analyze the existence of functional group after catalyst synthesis. H_2-TPR, CO_2-TPD and NH_3-TPD were conducted using a Micromeritics Chemisorb 2720 apparatus to examine the reducibility, basicity and acidity of the prepared catalysts. The details of these three analyses have been reported in our previous research [42, 43]. The weights of carbonaceous deposits on the spent catalysts were analyzed by thermogravimetric analysis (Perkin Elmer TGA). Spent catalysts were also analyzed by ICP, CHNS and BET surface area techniques to get more understanding of the coke deposition on the catalysts surface.

2.3 Catalytic activity in PET-phenol cracking and steam reforming

The reaction was accomplished in a fixed-bed reactor, loaded with 0.2 g of catalyst diluted with silicon carbide (2:3) to increase catalyst activity [1, 39]. The reaction was obtained using our previously reported procedure [35-38], and the schematic process flow diagram of the reactor system is shown in Figure 1. At the first step of the reaction, the PET source such as waste bottles was cut in 50 mm^2 pieces and melted in phenol whilst mixing at 90 ^oC. The bottle pieces were completely disappeared in the phenol even after cooling the mixture. The PET-phenol mixture then injected to the reactor by a syringe pump at 0.04 ml/min and water was injected to preheater via HPLC pump at 0.36 mL/min. Both water and PET-phenol mixture were vaporized at 200 ^oC using knitting in duo-tape heaters formerly entering the reactor with the 1:9 ratios. Before the reaction, the catalysts were reduced by H_2 flow at 600 ^oC for an hour. N_2 gas was introduced in the experiment as a carrier gas with a flow rate of 30 mL/min. At the same time, the feed was injected into the reactor by the syringe pump, and the reaction took place at 500-800 ^oC. The liquid product was examined by GC-FID (HP 5890 Series II), and the gas product was evaluated by an on-line GC-TCD (Agilent 6890N). The feed conversion and hydrogen yield were calculated using Equation 2 and Equation 3, respectively. The reaction rate by Arrhenius plots, kinetic constants and reaction orders were then calculated following our previous research [41].

$$\text{Conversion } (\%) = \frac{[\text{Feed}]_{\text{in}} - [\text{Feed}]_{\text{out}}}{[\text{Feed}]_{\text{in}}} \times 100\% \quad (2)$$

$$H_2 \text{ yield } (\%) = \frac{\text{moles of } H_2 \text{ obtained}}{\text{moles of } H_2 \text{ stochiometric potential}} \times 100 \quad (3)$$

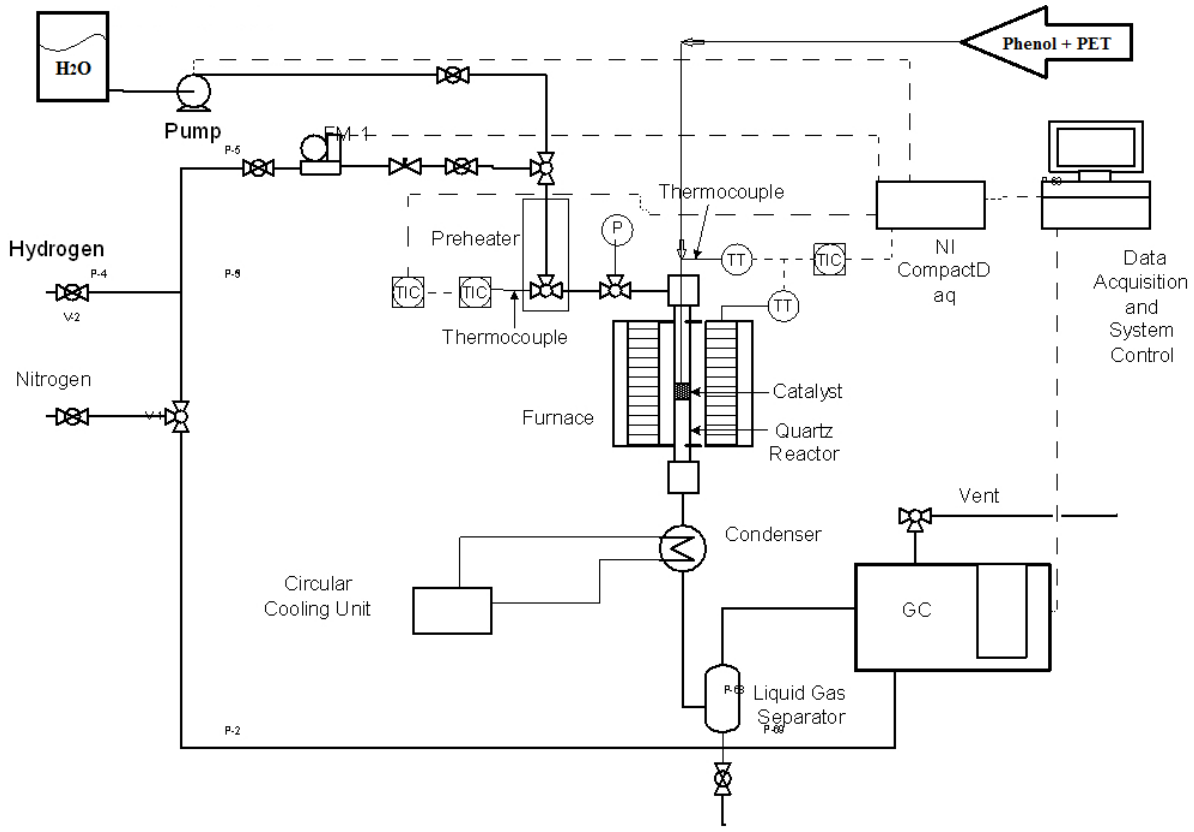

Figure 1 A schematic diagram of the catalytic steam reforming reactor

3 Results

3.1 Catalyst characterization

N_2 adsorption-desorption tests characterized the pore size distribution and specific surface area and of NC-Ce-imp and NC-Ce-hyd catalysts. Figure 2(a) shows the N_2 adsorption-desorption isotherms, and Figure 2(b) shows the pore size distributions. The specific surface area, pore volume and average pore diameter of the catalysts are also shown

in Table 1. At the table, the metal content was measured by ICP test, S_{BET} is the BET surface area, V_p, is the total pore volume, and D_p, is the average pore diameter of the catalysts. The adsorption-desorption of N_2 was well-expressed type IV isotherms, with a hysteresis loop arising at the area of the relative pressure of P/P_0=0.5–1.0 associated with the presence of macroporous structures [40]. Commonly, the mesoporous structure has efficient electron mobility and confinement effects, and this cause to outstanding properties in catalysis reactions. Figure 2(a) proves that the hysteresis loop presence and also the pore size distribution illustrates the catalysts are orderly mesoporous. The pore size distribution presented in Figure 2(b) shows that the pore diameters of NC-Ce-imp and NC-Ce-hyd are around 30 nm and 13 nm, respectively, which also confirms the mesoporous structures of the samples. The mesoporous properties obliged as a tunnel structure to enhance the interaction of plastic waste particles with the surface of the catalyst during the PET-phenol cracking and steam reforming process. Besides, the NC-Ce-imp mesopore that is lower than 20 nm were entirely vanished, subsequent in the more major pore development (~30 nm). In contrast, the creation of a large pore (~ 30nm) of NC-Ce-hyd is almost disappeared, resulting in the formation of a small mesopore (~13 nm).

The surface area of the NC-Ce-hyd nanosized catalyst (11.3 m^2/g) was approximately more than two times that of the NC-Ce-imp catalyst (4.4 m^2/g) supplemented by the rise of the pore volume from 0.0827 to 0.0961 cm^3/g. The possible reason for this low surface area can be the coverage of the support surface by active metals. A possible clarification is that the CeO_2 impassable a large amount the lowest pore diameters in the conventional impregnation method; consequently, the average pore diameter improved. Another possibility could exist associated with the reduction of the crystallite size of NC-Ce-hyd catalyst to roughly level. The catalyst activity improvement is aligned with the high specific surface area and pore

volume of NC-Ce-hyd nanosized catalyst, these advantages could increase the contact among reactant and catalyst surface. The large surface area displays various crystal facets, which are observed as the active sites for the waste elements adsorption; the NC-Ce-hyd nanosized catalyst could be an ideal choice for waste steam reforming reaction.

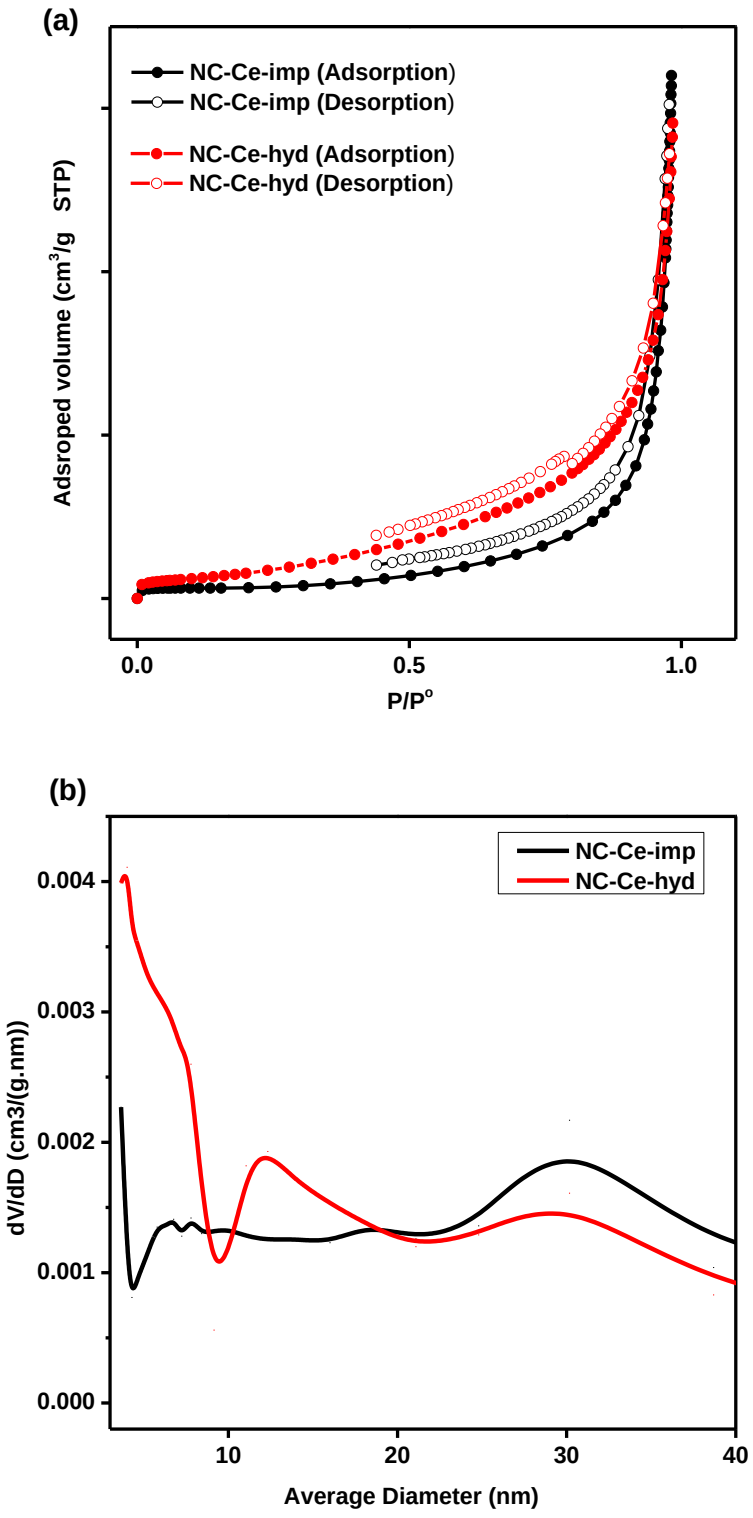

Figure 2 (a) Nitrogen adsorption isotherm and (b) pore size distribution of the fresh NC-Ce samples.

Table 1 Chemical composition, BET surface area, pore-volume, and average pore diameter of NC-Ce-imp and NC-Ce-hyd nanosized samples

	Ni (wt%)	Co (wt%)	Samples after reduction		
			S_{BET} (m^2/g)	V_p (cm^3/g)	D_p (nm)
NC-Ce-imp	5.97	3.99	4.4	0.0961	32.02
NC-Ce-hyd	5.96	3.98	11.3	0.0827	13.21

XRD technique was employed to identify the catalyst crystal phase. The XRD plot of the reduced NC-Ce-imp and NC-Ce-hyd nanostructured catalysts at 600 ^oC are shown in Figure 3. The X-ray signal is characterized by a variety of sharp peaks between angles of 20 and 70°. The X-ray diffraction pattern of the NC-Ce samples has a Bragg peak of 44.5°. This relates to the Ni^o. The appearance of metallic Ni^o can be ascribed to cubic structure [JCPDS 45-1027] and is consistent with prior studies [5, 33, 40, 42]. The metallic Co^o [JCPDS 01-1254] peak was also detected at 44.3, which is agreed to the previous investigation too [22, 28]. The appearance of metallic Ni^o and Co^o at the XRD pattern proves that both these active metal oxide were reduced to the metallic phase under the reduction process [9, 20, 30]. The virtual strength of XRD peaks of the supported catalysts hinged on the nature of metal oxide precursors that shaped through the calcination procedure [60]. In both NC-Ce-imp and NC-Ce-hyd nanostructured catalysts, the only single peak for active metal was identified. This proves the creation of bimetallic Ni-Co through the reduction [60]. The XRD patterns of both NC-Ce-imp and NC-Ce-hyd nanostructured catalysts produced in typical peaks amount placed at 2 theta of 28.4, 32.9°, 47.2° and 55.9° corresponding to (111), (200), (220) and (311) crystal planes of the fluorite structure (JCPDS 81-0792) of CeO_2 [46, 47]. However, the XRD analysis detected other peaks at 2θ=37.3° and 53.7° for NC-Ce-hyd nanostructured

catalyst. The XRD patterns of the of peaks located at 2θ of 37.3° and 53.7° corresponding to (200) and (220) crystal planes of the α-Ce face-centred cubic structure (JCPDS 78-0640) [25]. Olsen et al. [45] claim that the α-Ce structure is stable at high pressure, even above 5 GPa.

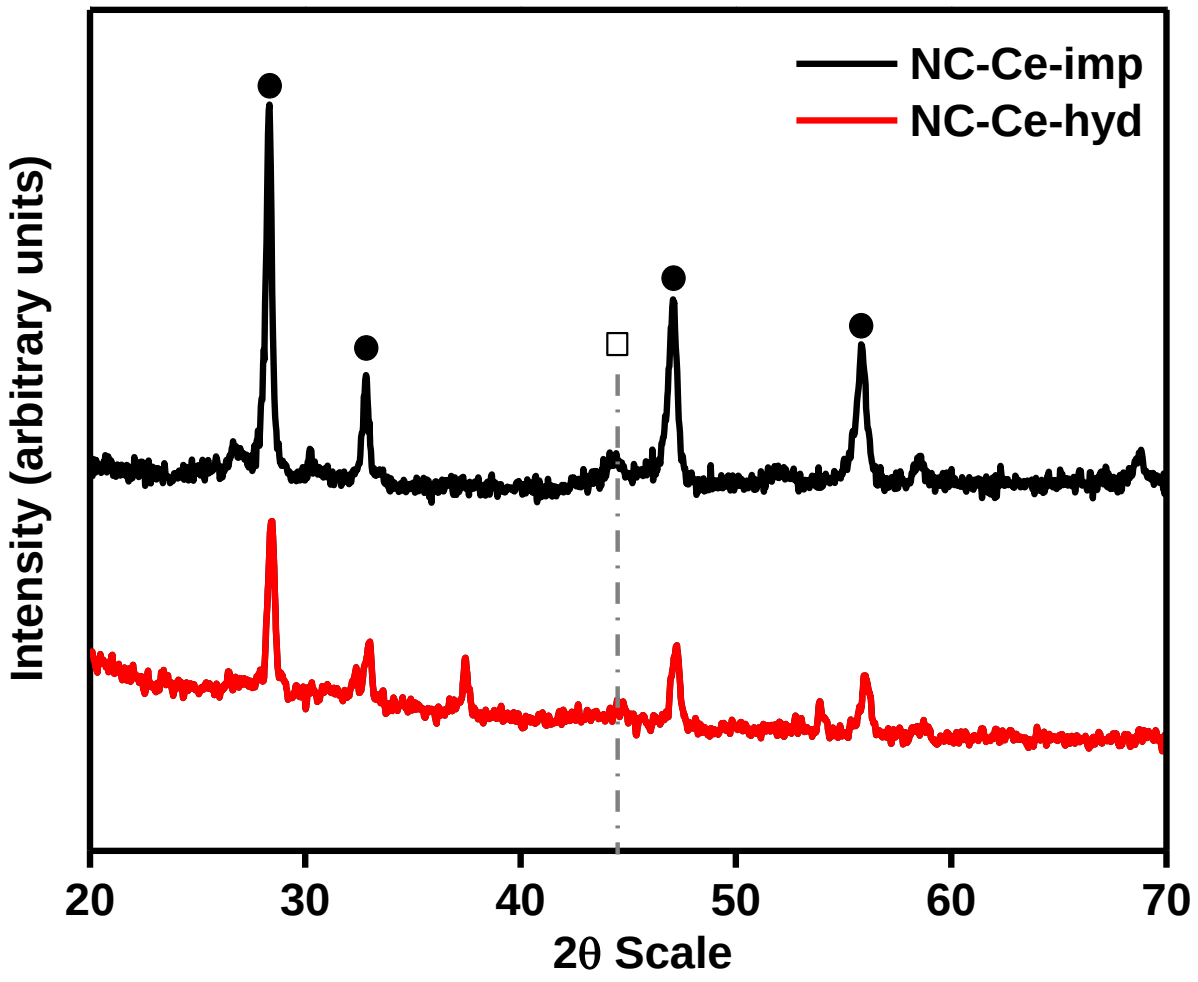

Figure 3 XRD profiles for NC-Ce-imp and NC-Ce-hyd nanosized catalysts after reduction at 600 °C

The surface morphologies of the NC-Ce-imp and NC-Ce-hyd are shown in Figure 4, and the d-spacing was calculated via Gatan Software (Gatan Microscopy Suite 2.1). The images reveal that a considerable amount of nickel with green arrows and cobalt with blue circles have been formed on both catalysts. There were some elements adsorbed on CeO_2, which can be guessed that nickel and cobalt particles were loaded on the CeO_2 surface. The precursor presents a sphere-like structure assembled from numerous nanosized particles. These shapes are interconnected to each other to form a network structure. Furthermore, it is noticed that high uniform and fine crystals have been prepared through a hydrothermal method. Compared to NC-Ce-imp, well-defined and smooth-surface sphere-like structures were found in NC-Ce-hyd. After hydrothermal preparation, the nanoparticles are stripped from the sphere-like structure, and NC-Ce-hyd nanoparticles are obtained. The figure presents that the morphology with uniform size distribution and the mean size of NC-Ce-hyd nanostructured catalyst was approximately 7 nm and lattice spacing equal to 0.383 nm (Co) and 0.184 nm (Ni) while of NC-Ce-imp was 12 nm with the lattice spacing's of 0.153 nm (Ni) and 0.12 nm (Co), without any significant agglomeration and the metal particles did not suffer from sintering and were separated well from each other.

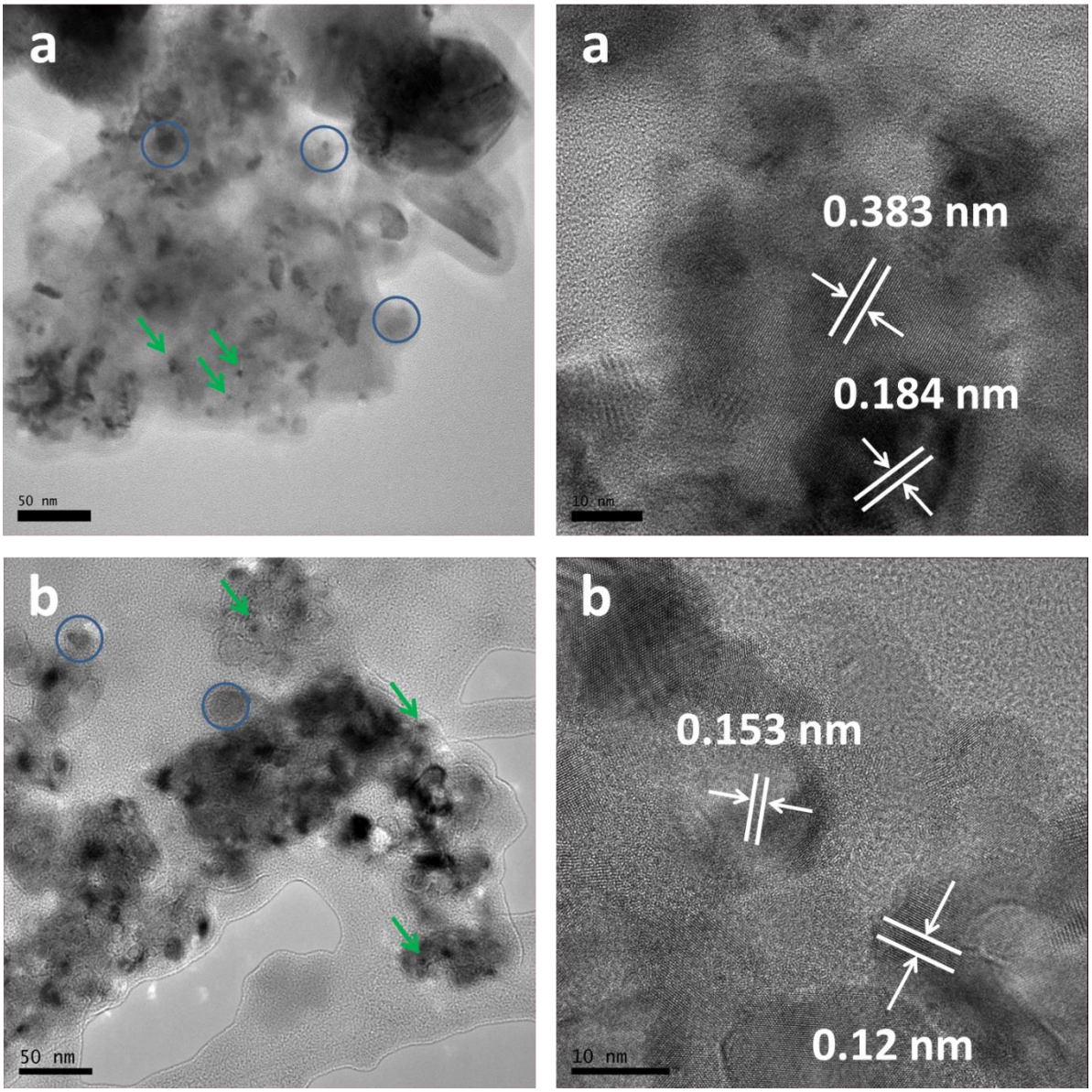

Figure 4 TEM images of (a) NC-Ce-imp and (b) NC-Ce-hyd nanosized samples.

The morphology and surface structures of the NC-Ce-imp and NC-Ce-hyd nanostructured catalysts are characterized by SEM and are shown in Figure 5a and Figure 5e. Homogenous active metal distribution on the support is delivered for both hydrothermal and conventional

impregnation methods. The representative SEM images of the NC-Ce catalysts is indicating that the NC-Ce-imp did not reveal any specific shape and looks like composed of agglomerated nanoparticles with various pore sizes ranging from 1 to 5 µm, while NC-Ce-hyd were unvaryingly spherical with a highly porous and rough surface with a different pore size of ~1 µm. In this means, the active phase of the NC-Ce-hyd nanostructured catalyst is in an appropriately great distributed form, which consequences in a large specific surface area and supposed to have maximum catalytic performance. It is very clear from the SEM study that preparation through hydrothermal treatment during the synthesis of bimetallic nanostructured catalysts results in the variation of their morphological features also. The EDX spectrum of NC-Ce-imp and NC-Ce-hyd nanostructured catalysts, as shown in Figure 5d and Figure 5h, further confirm that the Co, Ni, and Ce elements are present in both catalysts. The appearance peaks of these elements provide the evidence that bimetallic Ni-Co were successfully formed and deposited onto CeO_2. As can be seen from Figure 5, several elements, i.e., Co, Ni, and Ce, could be detected. The EDX data of different elements showed that the weight percent of Ni, Co, and Ce for the NC-Ce-imp catalyst was around 24.8, 23.8, and 51.4 while for the NC-Ce-hyd was 23.3, 20.6 and 56.1, respectively.

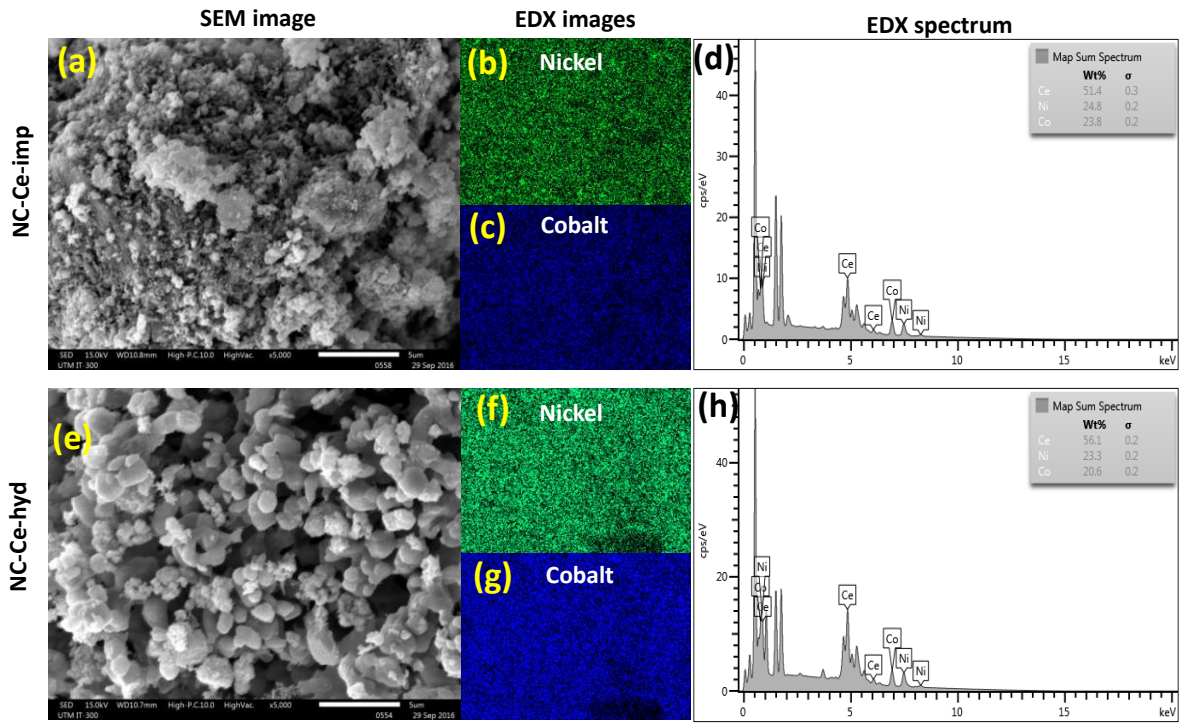

Figure 5 (a) Scanning Electron Microscopy (SEM) photo and (b, c, d) Energy dispersive X-ray (EDX) analysis of NC-Ce-imp, (e) SEM image (f, g, h) EDX analysis of NC-Ce-hyd nanosized catalyst.

To investigate practical clusters presents in the prepared catalysts the FTIR spectrum using the KBr pellet technique was recorded in the wavenumber ranging from 4000 to 500 cm^{-1}, as revealed in Figure 6. Peaks at ~1640 cm^{-1} can be ascribed to the asymmetrical extending mode of ν (O-H), and δ (O-H) from the surface adsorbed water and the broad peaks at high wavenumber about ~3450 cm^{-1} ascribed to the yielding vibration of physical O-H [55]. The negative bands situated at 3745 cm^{-1} might be attributed to loss of ν(OH) strength of diverse sorts of free hydroxyl groups formerly existing on the CeO_2 surface. FTIR spectra of the catalysts exhibited weak absorption around ~1076 cm^{-1} and shoulder at ~980 cm^{-1} due to the presence of residual nitrate moiety (ν (NO_3^-)) over CeO_2 surface and shoulder bellow ~980 cm^{-1} attributed to Ce-O stretching vibrational mode [57]. FTIR spectra that bellow the 1000 cm^{-1} are related to metal oxides arising from interatomic vibrations [52]. On NC-Ce-hyd

nanostructured catalyst, adsorption has a specified increase to a band at 1446 cm^{-1}. These bands are assignable to overtone O–H stretching mode [52]. The weak ν_2 band at around 879 cm^{-1} in the NC-Ce-hyd sample and 879 cm^{-1} in the NC-Ce-imp catalyst approve the existence of CO_3^{2-} [34] and to Co–OH modes. No other band was detected 980 cm^{-1} for the NC-Ce catalyst. It is due to the very small Ni–O crystals in the Ni-Co/CeO_2 nanostructured catalyst.

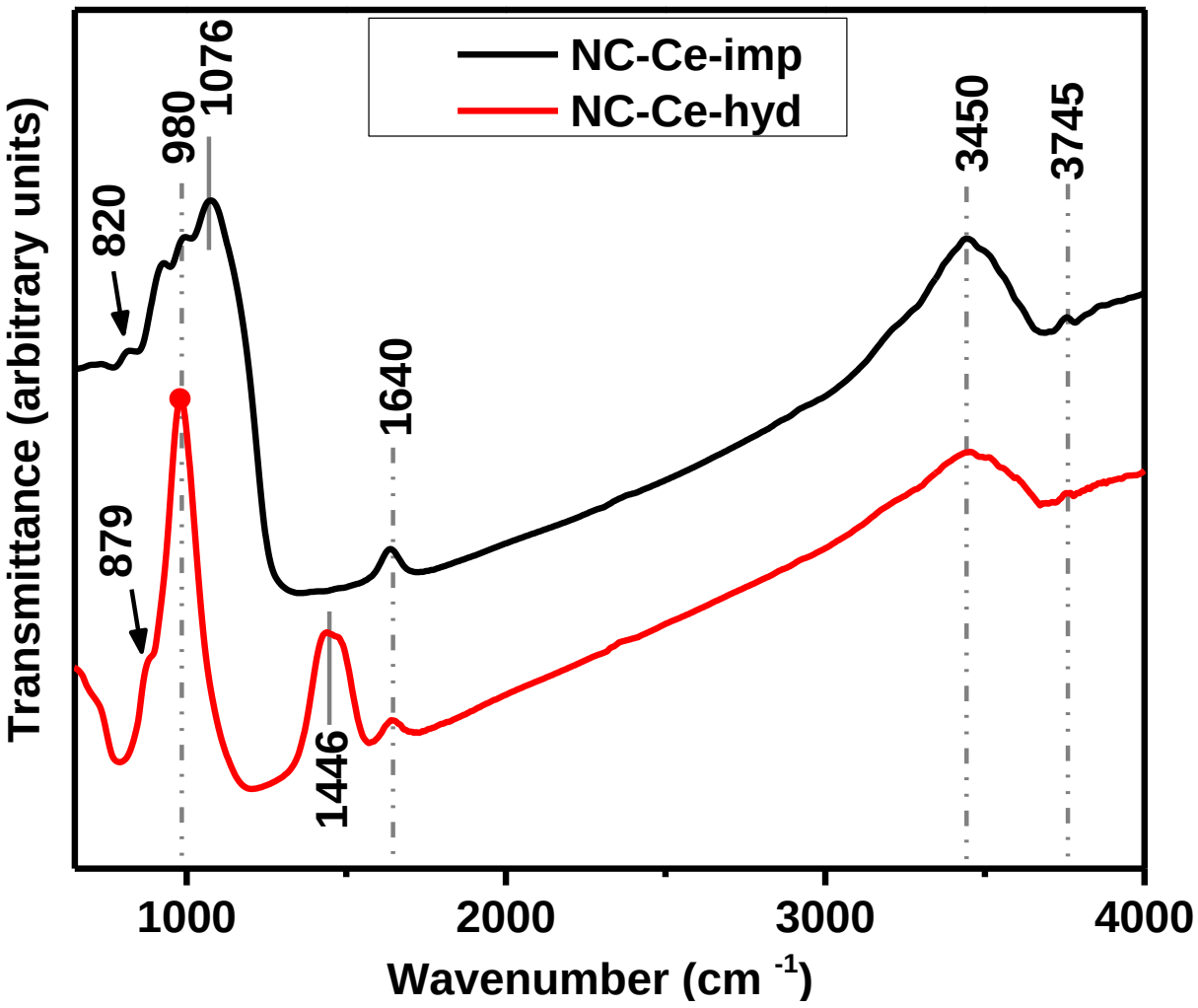

Figure 6 FTIR curves of NC-Ce-imp and NC-Ce-hyd nanosized samples.

TPR study was applied to investigate the behaviour of metal and support interaction. Moreover, TPR determines the behaviour of active metal during reduction reactions. The total H_2 consumption for each catalyst was correlated to the entire area underneath the H_2-TPR profiles. The H_2-TPR patterns of NC-Ce-imp and NC-Ce-hyd nanostructured catalysts were carried out on all catalysts after calcination at 800 °C before the reduction is shown in Figure 7. In general, reduction peaks at the low-temperature area (bellow 400 °C) are ascribed as the reduction of NiO and CoO to the metallic Ni and Co. This region also clarifies of weak interaction of metallic Ni and Co with CeO_2, as shown in Eq (4) and Eq (5).

$$NiO + H_2 \rightarrow Ni^0 + H_2O \quad (4)$$

$$CoO + H_2 \rightarrow Co^0 + H_2O \quad (5)$$

In particular, the amount of H_2 consumption of sub-peaks and reduction degree is shown in Figure 7. The incomplete reduction of CeO_2 is detected at the TPR pattern at ~350 ^oC [15] with the actual amount of 415.3 μmol/g. The prominent H_2 consumption peaks at 387 °C and 758 ^oC for NC-Ce-imp, accredited to the pure metal oxides and spinel oxides reduction, respectively. Notably, the spinel phase has a positive effect and catalytic reaction and can alleviate the creation of small size Ni metallic crystallites in reduction circumstances [6]. Another possibility of these two reduction areas could be attributed to diverse NiO components whose interaction level with the support is related to the escalation of temperature and oppositely relative to their crystal size. Therefore, small nickel oxide elements that have significant interactions with the CeO_2 are reduced at beyond 400 °C. For the NC-Ce-hyd nanostructured catalyst, the first peak at 324 °C had been attributed to the

non-stoichiometric surface reduction of Ni(or Co)$^{3+}$ to Ni(or Co)$^{2+}$ [21]. In contrast, the peak at 426 ^{o}C catalyst had been because of the reduction of "unreacted" NiO (or CoO) on the surface, where this NiO form was virtually unaffected by the support. However, no reduction peak at higher temperatures was observed for NC-Ce-hyd, which again suggests significant interface among the Co and Ni on CeO_2-supported bimetallic sample. Interestingly the reduction peak of the NC-Ce-hyd shifted in H_2 consumption to lower temperatures with the preparation with hydrothermal treatment indicating that the NC-Ce-hyd nanostructured catalyst needs lower temperatures to reduce. By comparing the H_2 consumption for the NC-Ce-imp and NC-Ce-hyd nanostructured catalysts, one can see an expected difference in the H2 consumption. However the decrease is too large to be explained not only by the bimetallic Ni-Co reduction alone. The explanation for the lower part of this decrease is that the reducibility of NC-Ce is decreased in the hydrothermal treatment. This is evidence of a synergistic interaction between metals and CeO_2, causing the reduction of NC-Ce-hyd at a lower temperature compared to NC-Ce-imp.

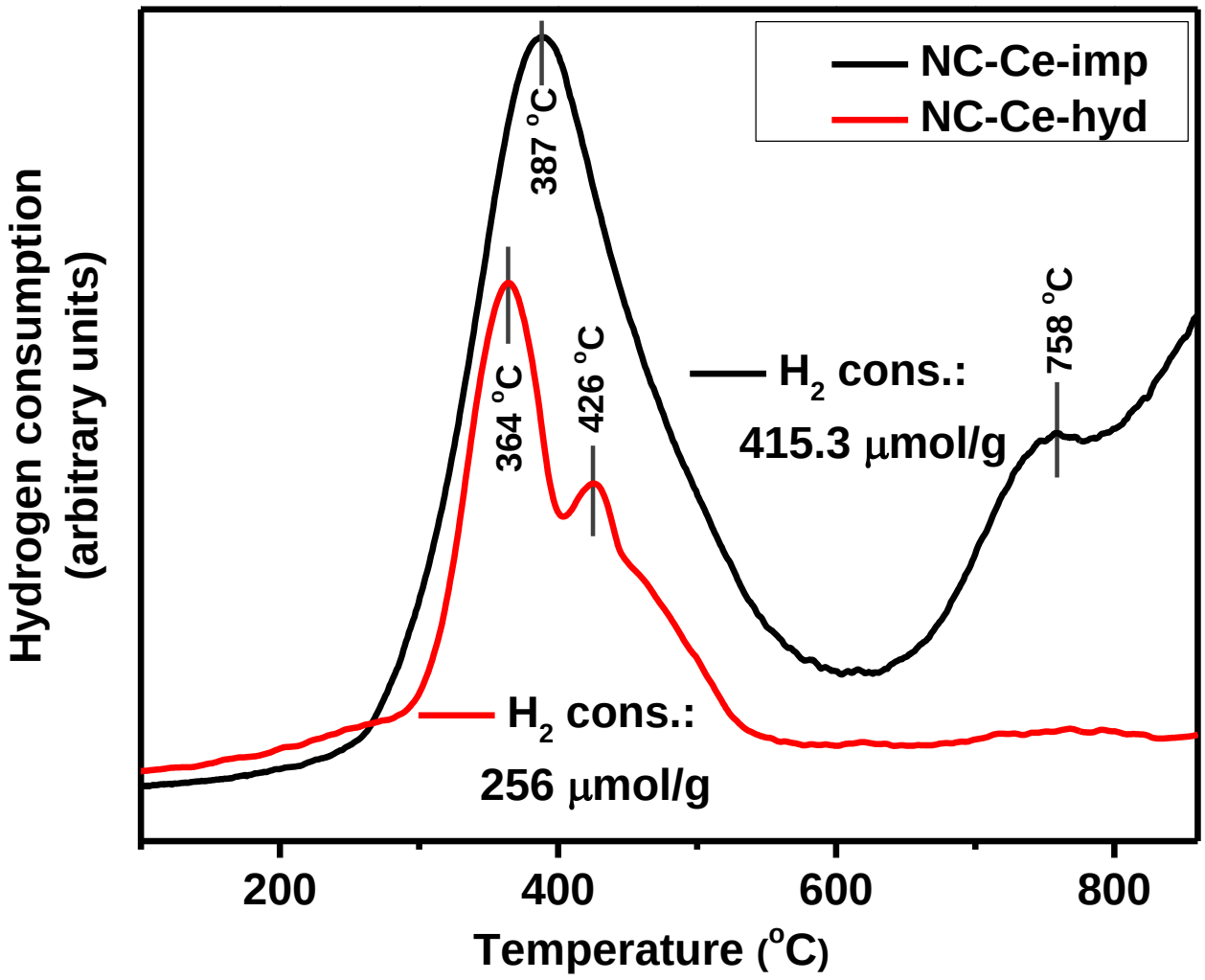

Figure 7 H_2-TPR profiles of NC-Ce-imp and NC-Ce-hyd nanosized samples.

To explain the total basicity and basic sites of materials, CO_2-TPD analysis was conducted. In general, the catalyst basicity strength and the basic quantity of catalysts can be calculated by the area under peaks, and CO_2-TPD profiles (after deconvolution) are shown in Figure 8. The CO_2 desorption peaks for the NC-Ce-hyd nanostructured catalyst occurring below the 100 °C (first peak), the range 250-400 °C (second peak) and 400-600 °C (third peak) are assumed to relate to CO_2 desorbing from weak, medium and strong basic sites, with

CO_2 uptake of 0.04, 0.6 and 1.43 μmol/g, respectively. The CO_2-TPD profile of the NC-Ce-imp catalyst indicates the weakness of this catalyst because of its weak basicity and basic amount. According to published research, CeO_2 [31, 63] support has OH^- (hydroxyl) groups in its constitution. Hence, the support weak basic sites might be the reason for hydrogen carbonates formation, which effects from particular interaction between the weak basicity of OH^- groups and CO_2 [19]. Besides, the coordination of metals through conventional impregnation preparation of the catalyst is the primary cause of the hydroxyl group formation. Thus the hydrothermal treatment will stop the formation of the hydroxyl group. It was stated that the catalytic selectivity and activity associates with the basic site strength and the basicity of the catalyst [18]. It is estimated that the hydrothermal treatment for NC-Ce-hyd nanostructured catalyst could have some influence on the catalytic activity and carbon deposition in PET-phenol cracking and steam reforming reactions.

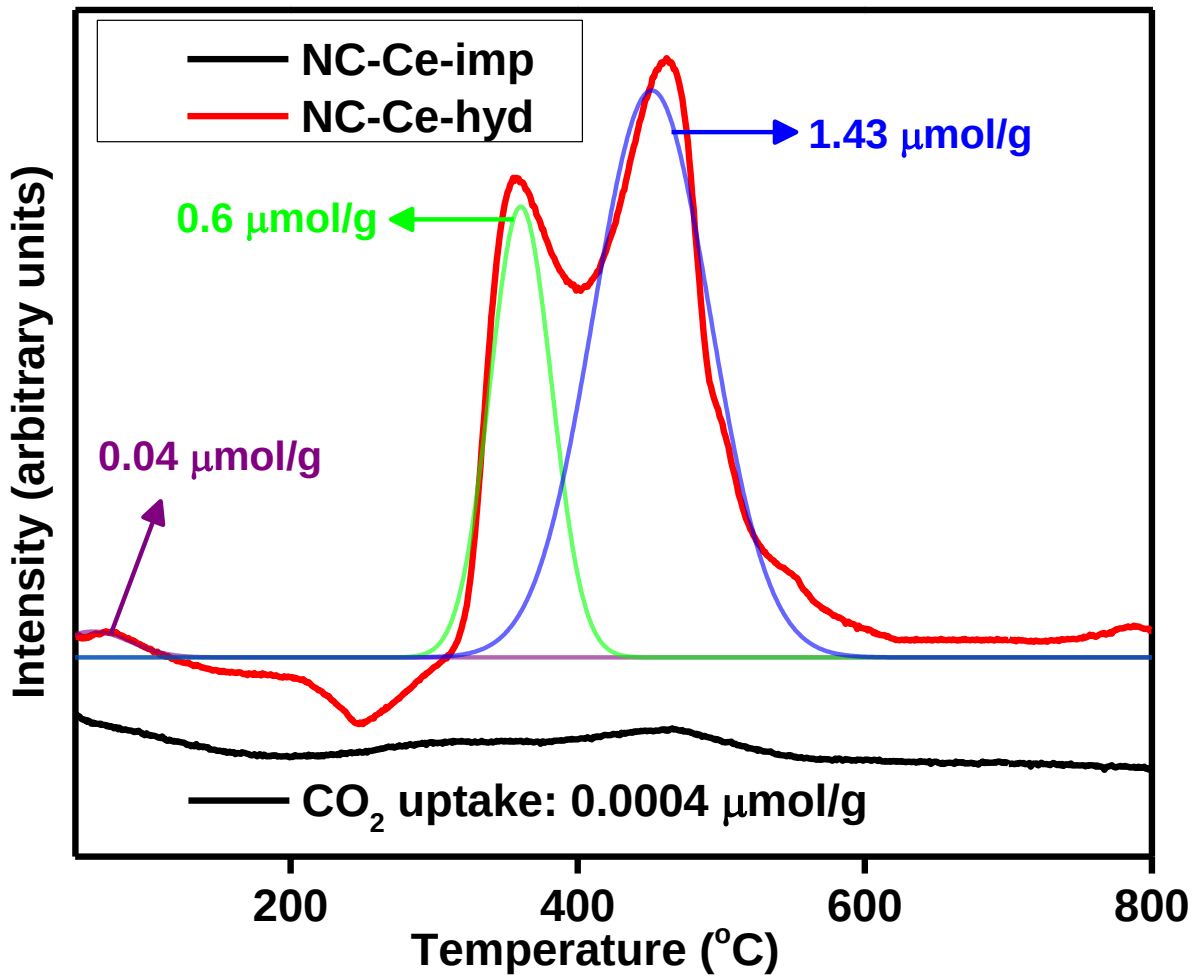

Figure 8 CO_2-TPD curves of NC-Ce-imp and NC-Ce-hyd nanosized samples.

The acidity of NC-Ce-imp and NC-Ce-hyd nanostructured catalysts was measured by NH_3-TPD, and findings (after deconvolution) are presented in Figure 9. NH_3 is a suitable examination molecule for analysis of solid materials acidity because of its acidity and tiny molecular volume, which tolerates NH_3 molecule to contact the acid sites even in microscopic pore [2]. The total medium and strong acid sites of the catalysts were calculated from the area below the corresponding NH_3 desorption peak and stated in the figure using different colours. It can be seen that the NC-Ce-imp catalyst did not gain any acidic site. The weak acidic sites of NC-Ce-imp may be associated with centers produced by the metal

assimilation [62] during the impregnation method. It can be seen that only NC-Ce-hyd catalyst possesses three desorption peaks at different temperature areas, deducing as the desorption medium acid sites at low-temperature region (100-400 °C) and strong acid sites at high-temperature region (> 400 °C). The high-temperature desorption peak (at 600 ºC) detected for the reveal the amount of NH_3 desorbed from strong metal cationic active sites. Besides, the deconvolution results display that the reduction temperature was increasing results in a higher amount of strong acid sites (0.67 µmol/g), probably because of the stronger Ni-Co interaction at higher temperatures.

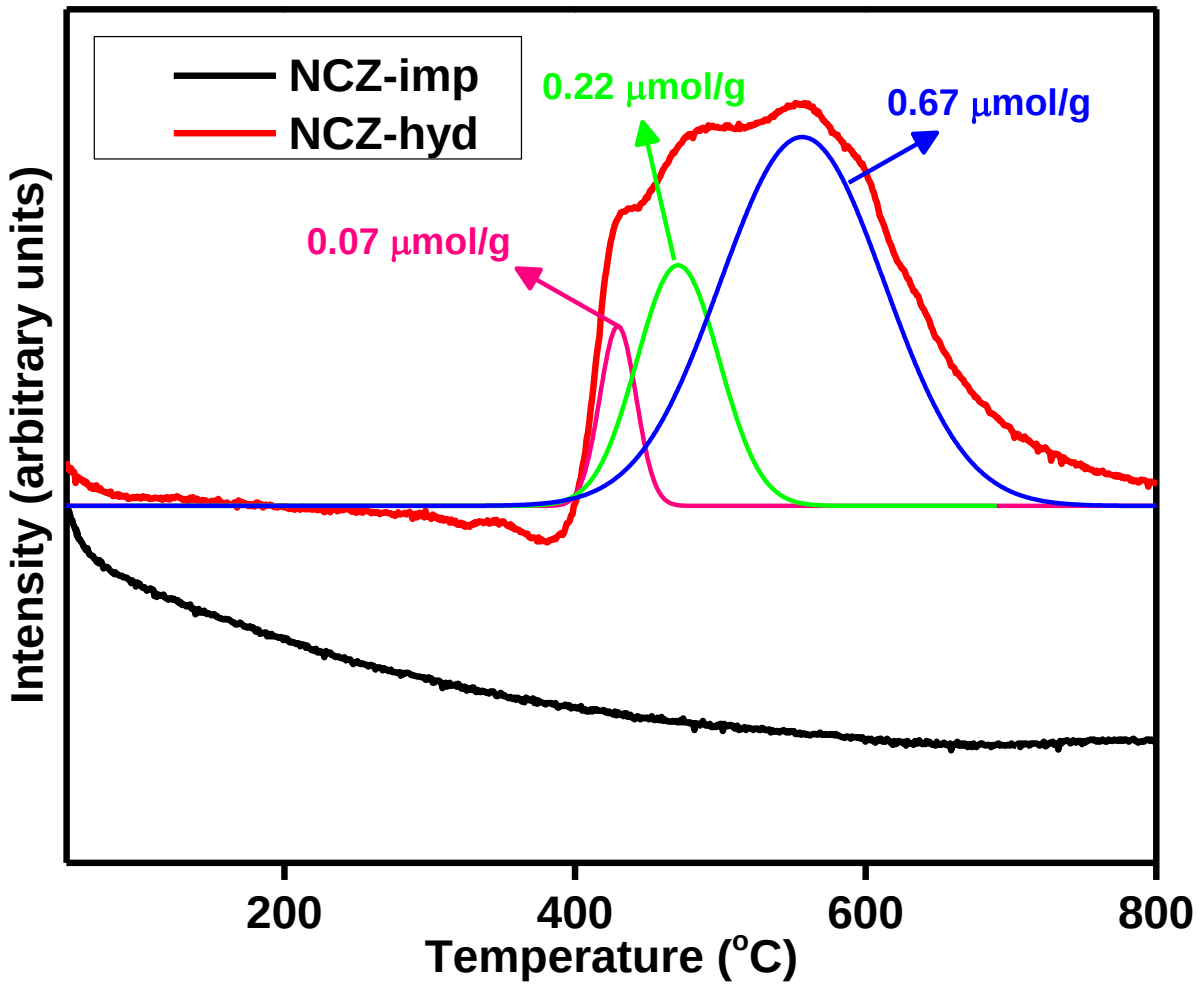

Figure 9 NH_3-TPD curves of NC-Ce-imp and NC-Ce-hyd nanosized samples.

3.2 Reaction study

To have more understanding of the impact of impregnation and hydrothermal synthesis of Ni-Co/CeO_2 nanostructured catalyst on the feed steam reforming reaction, catalytic tests at NC-Ce-imp and NC-Ce-hyd nanostructured catalysts were carried out. The operation conditions are described in section 2.3, and Figure 10 presents the catalytic performances at 500-800 °C. Generally, both of the NC-Ce-imp and NC-Ce-hyd nanostructured catalysts show an outstanding catalytic activity than a homogenous system which was without catalyst (not shown). As we can see that the feed conversion and hydrogen yield for both catalysts is increasing with temperature and is influenced by the diverse catalyst preparation techniques. The cleavage of the C-C bond and water gas shift reaction (Eq (8)) is controlling the reforming result. On the other hand, metals control the C-H and C-C bonds activation and support basicity are accountable for -OH and -H transfers. At the temperature above 700 ^{o}C for the NC-Ce-hyd nanostructured catalyst, the feed conversion escalation quickly and it becomes constant after 750 ^{o}C temperature, which displays that approximately complete conversion attained. This performance of the NC-Ce-hyd nanostructured catalyst can be defined by the hydrothermal treatment of the catalyst, which causes to create a high surface area, increase metals distribution uniformly and decrease the vulnerability to sintering. Khaled et al. [4] stated that the phenol steam reforming reaction is naturally endothermic, as shown in Eq (6) [54] and Eq (7) [44] and this cause the increase of hydrogen yield and phenol conversion by temperature.

$$C_6H_5OH + 11H_2O \leftrightarrow 6CO_2 + 14H_2 \qquad \Delta H^o = 463.65\ {}^{kJ}/_{mol} \qquad (6)$$

$$C_6H_5OH + 5H_2O \longrightarrow 6CO + 8H_2 \qquad \Delta H^o = 710.91\ {}^{kJ}/_{mol} \qquad (7)$$

$$CO + H_2O \leftrightarrow CO_2 + H_2 \qquad \Delta H^o = -41.15\ {}^{kJ}/_{mol} \qquad (8)$$

During the reforming reaction, the water gas shift reaction has a significant role in the hydrogen generation by taking CO molecules in attendance of steam. In this study, the CO and CO_2 contents are gradually decreased by temperature for both catalysts. This specifies that the water gas shift reaction is essential for achieving the desired feed conversion and hydrogen yield. It can be seen that the feed conversion and gas yield products were strongly affected by catalyst synthesis methods. For instance, the 600 ^oC temperature point illustrates 53.4% of feed conversion and 52.6% of hydrogen yield for the NC-Ce-imp catalyst, but these amounts were increased to 73.6% and 70.5% for feed conversion and hydrogen yield for the NC-Ce-hyd nanostructured catalyst, respectively. However, the waster gas shift reaction was raised at the same trend. According to XRD analysis in Figure 3, the NC-Ce-hyd detected the lower crystallinity than NC-Ce-imp but has proposed that the catalytic performance for NC-Ce-hyd sample has the more significant activity and selectivity towards feed conversion and gas product yield. This excellent activity for the NC-Ce-hyd sample is because of its higher basic sites and surface area, as shown in Table 1 and Figure 8, respectively. Morphological characterization also recommended that NC-Ce-hyd had the smallest metal particle size and resulted in great activity in the steam reforming and cracking reactions.

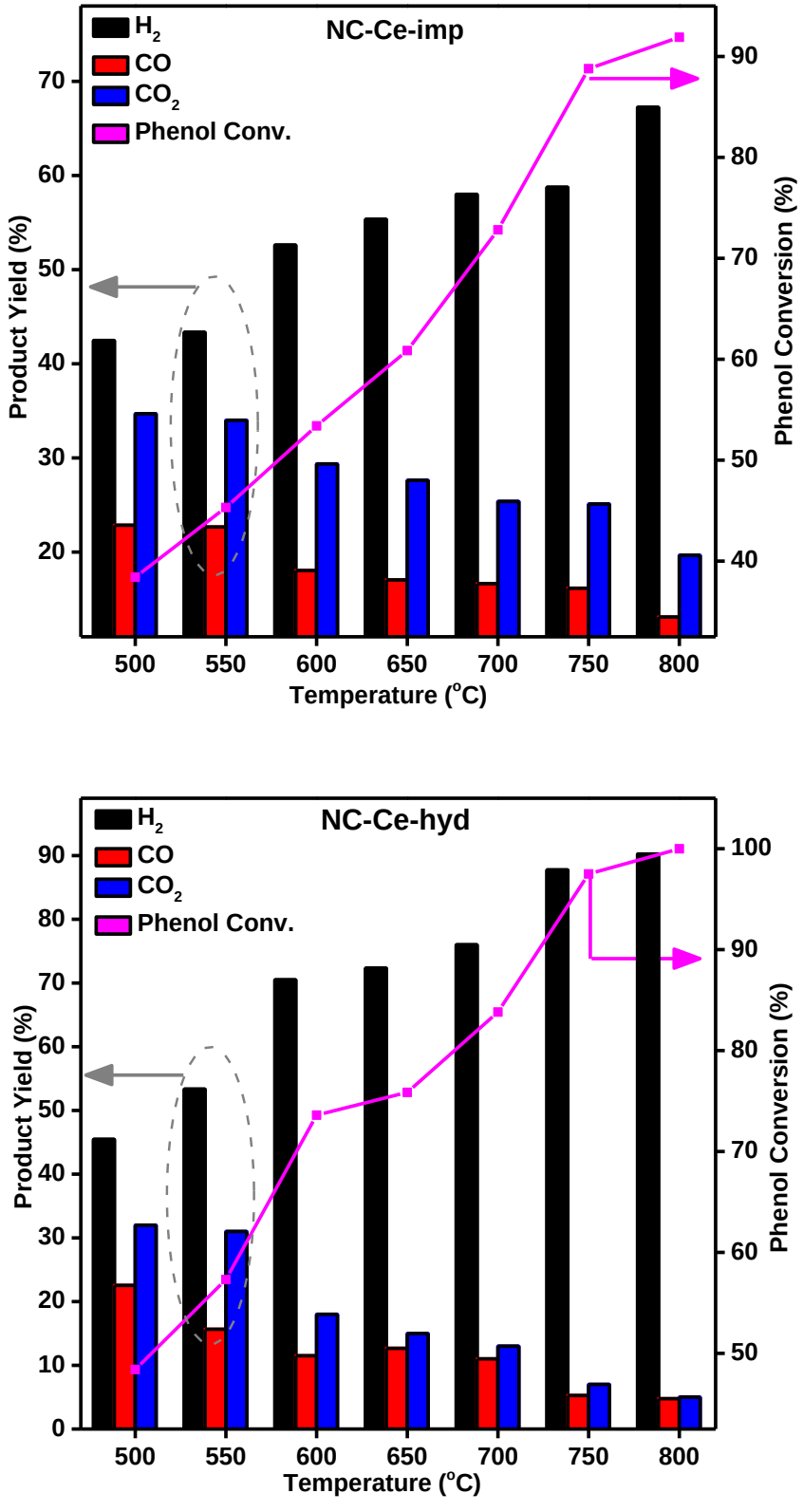

Figure 10 Phenol conversion and product yield of NC-Ce-imp and NC-Ce-hyd nanostructured catalysts.

The stability of NC-Ce-imp and NC-Ce-hyd nanostructured catalysts was assessed according to the times on stream 72 h (3 days) and illustrated in Figure 11. The assessment was considered as a function of feed conversion and hydrogen yield steadiness at 600 ºC. This temperature was selected for the catalyst stability test to avoid the possibility of thermal decomposition reaction at a higher temperature, which then decreases the accuracy of catalyst stability determination. There is probably coke deposition and formation as the steam reforming reaction of PET-phenol developed. This coke is in control catalyst deactivation and activity loss of catalytic site. The catalytic stability remarkably depends on the preparation methods. In specific, the primary carbon deposition on the catalyst surface plays a part in stability; in fact, it negatively changes the lifetime of the catalyst. As seen for the NC-Ce-imp catalyst in Figure 11, with the growth of time on stream (TOS), a significant catalyst deactivation was detected. Though, after almost 64 h time on stream, a nearly stable condition was achieved. The NC-Ce-imp catalyst was suffered from a progressive deactivation; the hydrogen yield and phenol conversion were decreased from 52.6% and 53.4% to 32.1% and 36.2%, respectively. This decrease in the NC-Ce-imp catalyst performance might be due to blocking the catalyst surface by carbon-containing species or the formation of by-product yields during the time on stream reaction. However, the NC-Ce-hyd sample displayed an outstanding stability and plateau performance during 3 days of reaction with no observing difference in gas products yields (the only hydrogen was shown). This achievement is possible because of the higher surface area and basic site of the NC-Ce-hyd nanostructured catalyst.

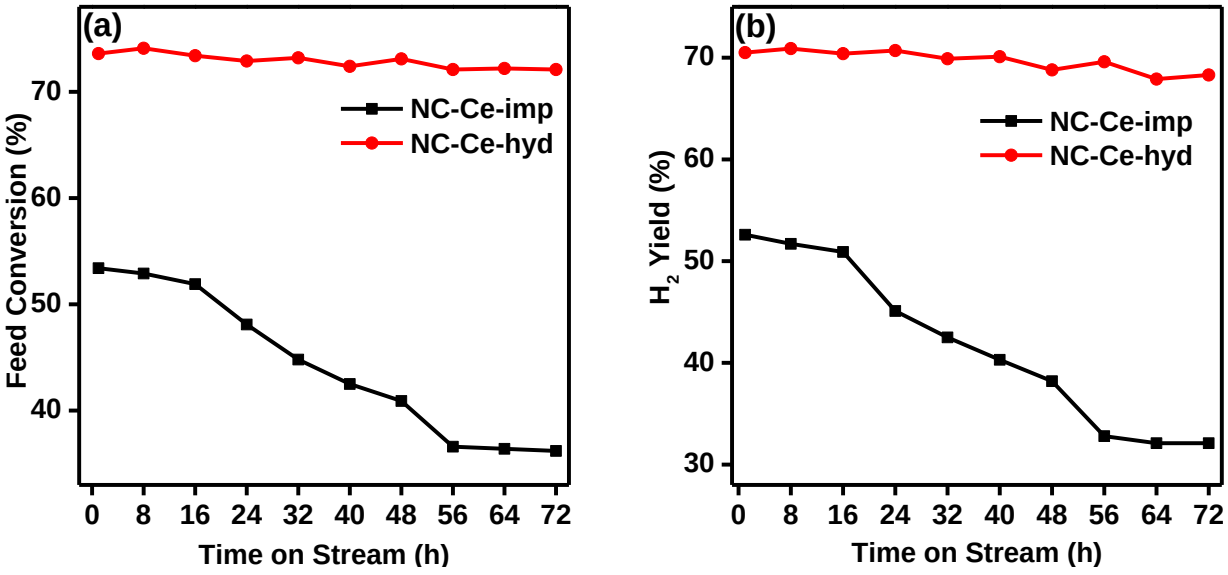

Figure 11 Stability of NC-Ce-imp and NC-Ce-hyd nanosized samples towards (a) feed conversion and (b) H_2 yield for three days of TOS

Figure 12 shows the activation energy (J/mol) that was measured via the Arrhenius plot under the hydrogen production and feed conversion at the temperature range of 500 ^{o}C to 800 ^{o}C. In general, the Arrhenius plots for both catalysts expose that the activation energies for H_2 generation are more than that for CO and CO_2, which means that H_2 is more temperature-sensitive than CO and CO_2. The higher activation energy required for NC-Ce-hyd catalyst for feed conversion and product yield can be ascribed to the shape of the reacted molecule on the surface of the catalyst. Al-Zuhair et al. [3] reported that the branched molecule increased the activation energy compare to linear molecules primarily because of the escalation in the diffusion activation energy. Therefore it is believed that the activation energy is affected by the chain length and structure. Consequently, the 43.58 J/mol and 106.2 J/mol of activation energy for hydrogen yield and feed conversion for the NC-Ce-hyd sample is due to the reaction of branched molecules. Table 2 displayed the kinetic constants and reaction orders that were calculated according to Equation 9 and following our previous study [41]. In this

equation, “r” is ascribed as the reaction rate and “a” and “b” symbols are attributed to the reaction order of phenol and water, respectively.

$$-r_{Ph} = kC_{Ph}^{a}C_{W}^{b} \quad (9)$$

As seen in Table 2, the reaction order for water molecules is zero, which indicates that the reaction rate is not dependent on water concentration. It can be concluded that the hydrothermal treatment can positively increase the reaction rate from 6.03 mmol/g_{cat}.s to 8.31 mmol/g_{cat}.s in comparison with the impregnation method.

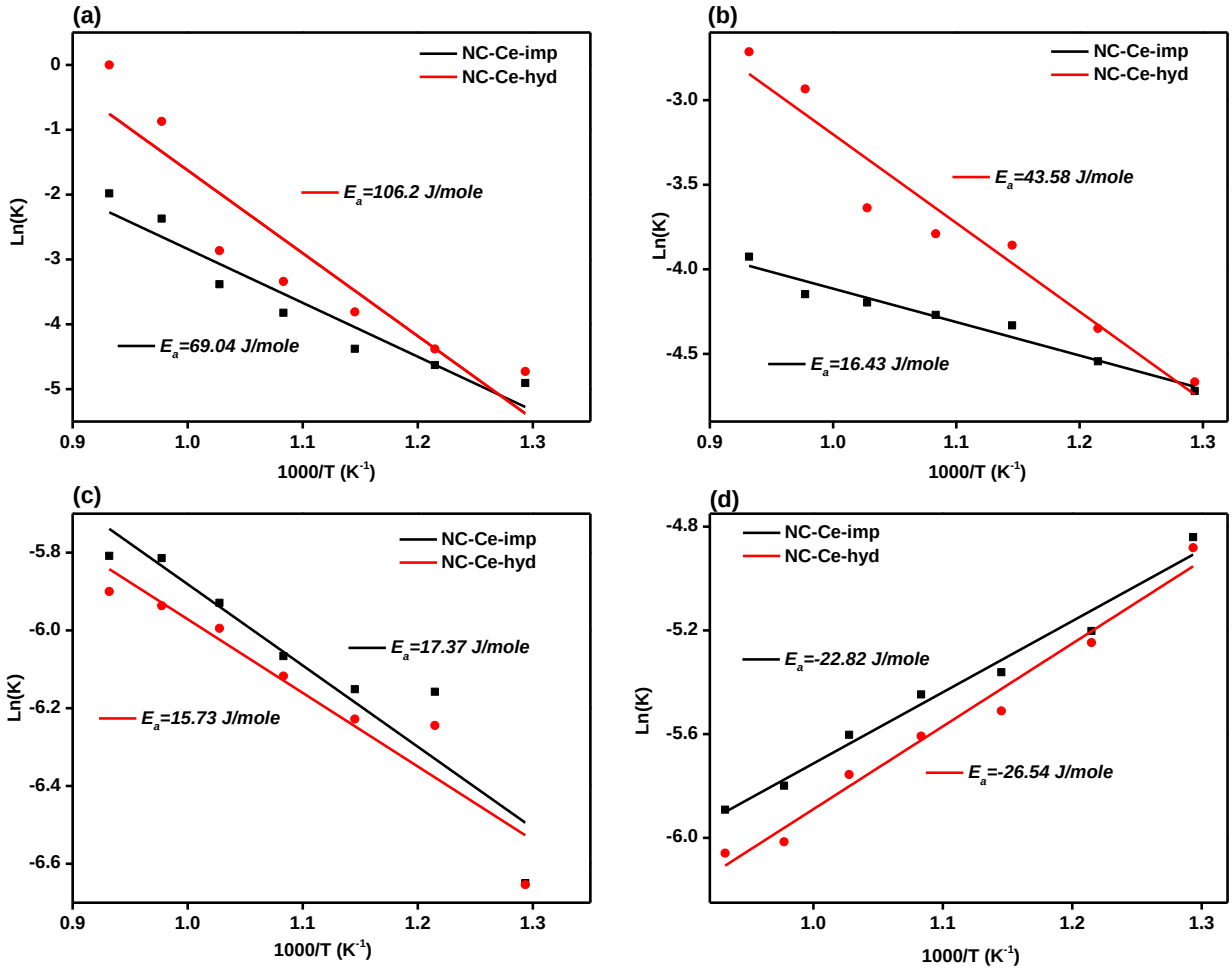

Figure 12 Arrhenius curve for feed steam reforming over the NC-Ce-imp and NC-Ce-hyd nanostructured catalysts for (a) phenol conversion, (b) H_2, (c) CO and (d) CO_2 yields in the temperature range of 500–800 °C

Table 2 The reaction order of and kinetic coefficients

Catalysts	$-r_{Ph}$ (mmol/g_{cat}.s)	k (s^{-1})	a	b	R^2
NC-Ce-imp	6.03	1.95	0.91	0	0.99
NC-Ce-hyd	8.31	14.7	0.98	0	0.96

R^2: optimization variable

3.3 Liquid Products Composition

The detected components from GC-MS analysis of liquid products from catalytic cracking of PET and steam reforming of phenol at 700 ^{o}C, together with their amount in percent, are shown in Table 3. Results display that the C_6H_5OH (phenol) component exists in the principal amount because of the phenol solvent used for PET dissolution. The big polymer compounds which did not comply with the cracking reaction were named as unidentified compounds. The compounds that are detected in the GC-MS analysis were split into four categories, such as aliphatics, naphthalenes, aromatics, and unidentified as obtained by published research [56, 58, 64]. Catalytic cracking of PET and steam reforming of phenol seems to produce valuable chemicals such as C_6H_6 (benzene) for both catalysts at almost the same amount of 0.05 and 0.06%. Other valuable components such as CH_3COOH (acetic acid), $C_8H_8O_2$ (phenyl ester), $C_{12}H_{10}O$ (diphenyl ether), $C_{13}H_{12}$ (2-methylbiphenyl), $C_{15}H_{16}O$ (1,1-diphenyl-2-propanol), $C_{13}H_{10}$ (Fluorene), $C_{13}H_{10}O$ (benzophenone), $C_{14}H_{10}$ (phenanthrene), $C_{18}H_{14}$ (o-Terphenyl) and $C_{16}H_{10}$ (pyrene) were also detected. The depolymerization of PET might have two-step mechanisms for benzene production; polyenes formation followed by benzene production. The dominant liquid products in the catalytic cracking of PET and steam reforming of phenol reactions were $C_{12}H_{10}$ (2-ethenylnaphthalene), $C_{12}H_8O$ (dibenzofuran), and C_8H_8O (acetophenone). At the NC-Ce-imp sample, there was a growth in unidentified components that specified that the NC-Ce-imp sample cause to produce of further important hydrocarbon. The branched-chained displayed a developed aliphatic quantity at both catalysts. Moreover, branched-chained compounds

display in a higher amount at NC-Ce-hyd nanostructured catalysts. This specified the creation of branched-chained radicals was desirable in PET cracking. The acidity and pore size properties of the catalyst play a significant role in the PET cracking. It was found that substantial cyclic composites and aliphatic in the range of C_4–C_8 produce from the cracking of PET. Besides, there was not any intermolecular transfer of hydrogen molecule to the cracked intermediates. Accordingly, these components were typically unsaturated. It should be noted that the NC-Ce-imp has a lower concentration of phenol but the higher content of C_7H_8O (2-methyl phenol), dibenzofuran, compared with the NC-Ce-hyd catalyst.

Table 3 Liquid Products

Compound	Without catalyst	NC-Ce-imp	NC-Ce-hyd
C_6H_6	0	0.06	0.05
C_6H_5OH	93.4	91.1	90.92
CH_3COOH, $C_8H_8O_2$	0	0.06	0.08
C_7H_8O	0	0.12	0.09
C_8H_8O	0	0.15	0.18
$C_{10}H_8$	0	0.09	0.13
$C_{12}H_{10}$	0	0.23	0.24
$C_{12}H_{10}O$	0	0.05	0.05
$C_{13}H_{12}$	0	0.03	0.06
$C_{15}H_{16}O$	0	0.01	0.03
$C_{12}H_8O$	0	0.33	0.16
$C_{13}H_{10}$	0	0.03	0.03
$C_{13}H_{10}O$	0	0.01	0.03
($C_{14}H_{10}$	0	0.02	0.09
$C_{18}H_{14}$	0	0.02	0.01
$C_{16}H_{10}$	0	0.03	0.03
Unidentified	6.6	7.66	7.82
Total	100	100	100

3.4 TGA analysis

Thermogravimetric analysis (TGA) tests were conducted to investigate the thermal stability by defining the volume of the carbon deposition on the catalyst surface after reaction at 600 °C. The percentage of weight loss curves as a temperature function were plotted in Figure 13 and quantity deposited coke, weight loss, carbon content (CHNS elemental analysis), metal content (ICP test) and the spent catalysts surface area are reported in Table 4. Weight loss at WL_1 was observed in both catalysts. The loss of weight probably is caused by trapped water molecules. At this temperature, the weight loss of the NC-Ce-imp catalyst is considered as high. Besides, such extreme temperature could burn some trapped hydrocarbons; hence, it exhibits a higher weight loss. It can be seen that the weight loss of the NC-Ce-imp catalyst at the WL_2 area was 2.47%; this might suggest the presence of further amorphous carbon for the latter, which is gasified at lower temperatures associated with filamentous carbon that is probably dumped on NC-Ce-hyd. Interestingly, not only the NC-Ce-hyd catalyst did not suffer from carbon deposition on its surface but also exhibited weight gain. Previous research [16, 61] has claimed that this weight gain may be because of the oxidation of the metallic active sites. Furthermore, NC-Ce-hyd catalysts had a lower overall weight loss of 6.92%, compared to the NC-Ce-imp catalyst that shows a weight loss of 8.24%. The CHNS analysis proves the trend of the TGA profile as well in which the carbon content of NC-Ce-hyd catalyst (3.7%) is almost half of the carbon content of NC-Ce-imp one (6.1%). ICP and BET tests show that the metal content and the surface area of the NC-Ce-imp catalyst decreased more than the NC-Ce-hyd catalyst. NC-Ce-hyd sample with the best catalytic activity presented the minimum mass loss during the PET-phenol steam reforming reaction, suggesting its high potential for coking resistance. Moreover, the TGA results showed a reasonable agreement with that of CO_2-TPD and catalyst activity evaluation. Therefore the hydrothermal treatment plays an important role in basicity and coke deposition. The basicity of NC-Ce-hyd may result in less amount of carbon deposition and excellent

reaction performance, which sufficiently proved that suitable catalyst preparation could fundamentally improve the catalytic activity and stability.

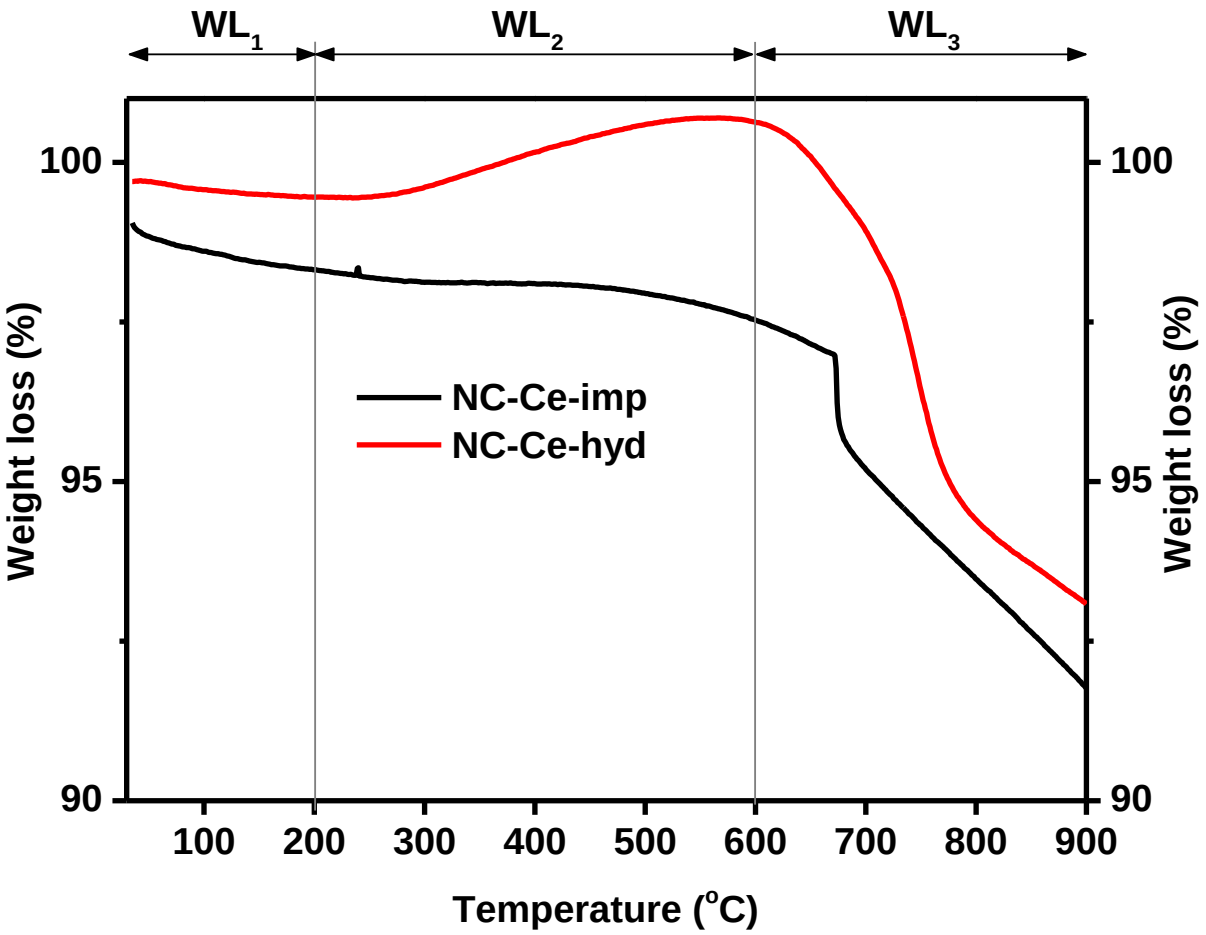

Figure 13 TGA curve of NC-Ce-imp and NC-Ce-hyd nanostructured catalyst

Table 4 Weight loss, carbon and metal contents and surface area of the samples after reaction

Catalysts	Weight loss (%)	Total weight loss (%)	Ni (wt%)	Co (wt%)	Carbon Content (wt.%)	S_{BET} (m^2/g)[a]

	WL_1	WL_2	WL_3					
NC-Ce-imp	1.68	0.79	5.77	8.24	4.82	2.97	6.1	2.9
NC-Ce-hyd	0.54	0	6.92	6.92	5.43	3.58	3.7	10.6

[a] S_{BET}, BET surface area

4 Conclusion

The cracking and the steam reforming reactions of PET-phenol for hydrogen and valuable fuel production was conducted using NC-Ce-imp and NC-Ce-hyd nanostructured catalysts. In summary, the findings revealed that the hydrothermal preparation method plays an essential role in pore sizes, level of metals interaction with support compounds, and physiochemical properties, playing a different effect on the catalytic performances of Ni-Co/CeO_2 catalysts. With the content of different preparation methods, the particle size on the catalysts was reduced for the NC-Ce-hyd catalyst. In combination with the TEM image findings, it was achieved that hydrothermal treatment can decrease the metal compounds particle size, which approved that the dispersion of metal elements was enhanced. Both basicity and acidity properties of catalysts were enhanced for NC-Ce-hyd nanostructured catalyst, which leads to improve in the hydrogen yield, phenol conversion, and reaction rate in comparison to NC-Ce-imp catalyst. The hydrothermal treatment has an excellent promotional effect for the resistance to coke deposition and catalyst stability as well. More remarkably, prised liquid products such as methyl phenol, benzene, dibenzofuran, acetic acid, 2-methylbiphenyl ,1,1-diphenyl-2-propanol, fluorene, pyrene and several other compounds

were produced after PET cracking and phenol steam reforming reactions. The findings of this research give a simple and effective method for the development of anti-sintering, carbon-resistant bimetallic Ni-Co/CeO_2 nanosized catalyst for the generation of hydrogen and valuable fuel from catalytic cracking of plastic wastes and steam reforming of phenol reactions.

Acknowledgement

The primary author, Walid Nabgan, is thankful for the support from Universiti Teknologi Malaysia in the form of the Post-Doctoral Fellowship Scheme "Development of a New Catalyst from a Waste to Produce Biodiesel" (PDRU Grant number: 04E81). The authors acknowledge the financial support given for this work by Universiti Teknologi Malaysia (UTM) under the Collaborative Research Grant (CRG) number 07G61, 07G59 and 07G62.

References

[1] Tuan Amran Tuan Abdullah, Walid Nabgan, Mohd Johari Kamaruddin, Ramli Mat, Anwar Johari, and Arshad Ahmad, 'Hydrogen Production from Acetic Acid Steam Reforming over Bimetallic Ni-Co on La2o3 Catalyst- Effect of the Catalyst Dilution', *Applied Mechanics and Materials*, 493 (2014), 39-44. https://doi.org/10.4028/www.scientific.net/AMM.493.39

[2] Muflih A. Adnan, Sagir Adamu, Oki Muraza, and Mohammad M. Hossain, 'Fluidizable Nio–Fe2o3/Sio2–Γal2o3 for Tar (Toluene) Conversion in Biomass Gasification', *Process Safety and Environmental Protection*, 116 (2018), 754-62. https://doi.org/10.1016/j.psep.2017.12.021

[3] S. Al-Zuhair, M. Hassan, M. Djama, and A. Khaleel, 'Hydrogen Production by Steam Reforming of Commercially Available Lpg in Uae', *Chemical Engineering Communications*, 204 (2017), 141-48. 10.1080/00986445.2016.1245186

[4] Khaled Saeed Baamran, and Muhammad Tahir, 'Ni-Embedded Tio2-Zntio3 Reducible Perovskite Composite with Synergistic Effect of Metal/Support Towards Enhanced

H2 Production Via Phenol Steam Reforming', *Energy Conversion and Management*, 200 (2019), 112064. https://doi.org/10.1016/j.enconman.2019.112064

[5] Elvin R. Beach, Krenar Shqau, Samantha E. Brown, Steven J. Rozeveld, and Patricia A. Morris, 'Solvothermal Synthesis of Crystalline Nickel Oxide Nanoparticles', *Materials Chemistry and Physics*, 115 (2009), 371-77. http://dx.doi.org/10.1016/j.matchemphys.2008.12.018

[6] M. Benito, S. García, P. Ferreira-Aparicio, L. García Serrano, and L. Daza, 'Development of Biogas Reforming Ni-La-Al Catalysts for Fuel Cells', *Journal of Power Sources*, 169 (2007), 177-83. http://dx.doi.org/10.1016/j.jpowsour.2007.01.046

[7] Xiaoyi Bi, Peng Wang, and Hong Jiang, 'Catalytic Activity of Cuon–La2o3/Γ-Al2o3 for Microwave Assisted Clo2 Catalytic Oxidation of Phenol Wastewater', *Journal of Hazardous Materials*, 154 (2008), 543-49. http://dx.doi.org/10.1016/j.jhazmat.2007.10.069

[8] Quan Bu, Kun Chen, Wei Xie, Yuanyuan Liu, Mengjie Cao, Xianghai Kong, Qiulu Chu, and Hanping Mao, 'Hydrocarbon Rich Bio-Oil Production, Thermal Behavior Analysis and Kinetic Study of Microwave-Assisted Co-Pyrolysis of Microwave-Torrefied Lignin with Low Density Polyethylene', *Bioresource Technology*, 291 (2019), 121860. https://doi.org/10.1016/j.biortech.2019.121860

[9] Moisés Cabo, Sebastiano Garroni, Eva Pellicer, Chiara Milanese, Alessandro Girella, Amedeo Marini, Emma Rossinyol, Santiago Suriñach, and Maria Dolors Baró, 'Hydrogen Sorption Performance of Mgh2 Doped with Mesoporous Nickel- and Cobalt-Based Oxides', *International Journal of Hydrogen Energy*, 36 (2011), 5400-10. http://dx.doi.org/10.1016/j.ijhydene.2011.02.038

[10] Javier Carrasco, Laura Barrio, Ping Liu, José A Rodriguez, and M Veronica Ganduglia-Pirovano, 'Theoretical Studies of the Adsorption of Co and C on Ni (111) and Ni/Ceo2 (111): Evidence of a Strong Metal–Support Interaction', *The Journal of Physical Chemistry C*, 117 (2013), 8241-50.

[11] Yue Chai, Ningbo Gao, Meihong Wang, and Chunfei Wu, 'H2 Production from Co-Pyrolysis/Gasification of Waste Plastics and Biomass under Novel Catalyst Ni-Cao-C', *Chemical Engineering Journal*, 382 (2020), 122947. https://doi.org/10.1016/j.cej.2019.122947

[12] Domna A. Constantinou, M. Consuelo Álvarez-Galván, José Luis G. Fierro, and Angelos M. Efstathiou, 'Low-Temperature Conversion of Phenol into Co, Co2 and H2 by Steam Reforming over La-Containing Supported Rh Catalysts', *Applied Catalysis B: Environmental*, 117–118 (2012), 81-95. http://dx.doi.org/10.1016/j.apcatb.2012.01.005

[13] Haoran Ding, Cong Luo, Xiaoshan Li, Dingshan Cao, Qiuwan Shen, and Liqi Zhang, 'Development of Basrco-Based Perovskite for Chemical-Looping Steam Methane Reforming: A Study on Synergistic Effects of a-Site Elements and Ceo2 Support', *Fuel*, 253 (2019), 311-19. https://doi.org/10.1016/j.fuel.2019.04.150

[14] Changqing Fang, Ying Zhang, Ruien Yu, Xiaolong Liu, Jingbo Hu, and Maorong Zhang, 'Effect of Organic Montmorillonite on the Hot Storage Stability of Asphalt Modified by Waste Packaging Polyethylene', *Journal of Vinyl and Additive Technology*, 21 (2015), 89-93. 10.1002/vnl.21376

[15] R. Fiorenza, L. Spitaleri, A. Gulino, and S. Scire, 'Ru-Pd Bimetallic Catalysts Supported on Ceo2-Mnox Oxides as Efficient Systems for H-2 Purification through Co Preferential Oxidation', *Catalysts*, 8 (2018). 10.3390/catal8050203

[16] Germán Sierra Gallego, Jaime Gallego Marín, Catherine Batiot-Dupeyrat, Joël Barrault, and Fanor Mondragón, 'Influence of Pr and Ce in Dry Methane Reforming Catalysts Produced from La1−Xaxnio3−Δ Perovskites', *Applied Catalysis A: General*, 369 (2009), 97-103. http://dx.doi.org/10.1016/j.apcata.2009.09.004

[17] Lucía Garcia, Richard French, Stefan Czernik, and Esteban Chornet, 'Catalytic Steam Reforming of Bio-Oils for the Production of Hydrogen: Effects of Catalyst Composition', *Applied Catalysis A: General*, 201 (2000), 225-39. http://dx.doi.org/10.1016/S0926-860X(00)00440-3

[18] Vidya Sagar Guggilla, Jale Akyurtlu, Ates Akyurtlu, and Isaiah Blankson, 'Steam Reforming of N-Dodecane over Ru−Ni-Based Catalysts', *Industrial & Engineering Chemistry Research*, 49 (2010), 8164-73. 10.1021/ie100811g

[19] Elif I. Gürbüz, Edward L. Kunkes, and James A. Dumesic, 'Integration of C–C Coupling Reactions of Biomass-Derived Oxygenates to Fuel-Grade Compounds', *Applied Catalysis B: Environmental*, 94 (2010), 134-41. http://dx.doi.org/10.1016/j.apcatb.2009.11.001

[20] Seung Ju Han, Yongju Bang, Jaekyeong Yoo, Jeong Gil Seo, and In Kyu Song, 'Hydrogen Production by Steam Reforming of Ethanol over Mesoporous Ni–Al2o3–Zro2 Xerogel Catalysts: Effect of Nickel Content', *International Journal of Hydrogen Energy*, 38 (2013), 8285-92. http://dx.doi.org/10.1016/j.ijhydene.2013.04.141

[21] J. G. Highfield, A. Bossi, and F. S. Stone, 'Dispersed-Metal/Oxide Catalysts Prepared by Reduction of High Surface Area Oxide Solid Solutions', in *Studies in Surface Science and Catalysis*, ed. by P. Grange G. Poncelet and P. A. JacobsElsevier, 1983), pp. 181-92.

[22] J. C. Ingersoll, N. Mani, J. C. Thenmozhiyal, and A. Muthaiah, 'Catalytic Hydrolysis of Sodium Borohydride by a Novel Nickel–Cobalt–Boride Catalyst', *Journal of Power Sources*, 173 (2007), 450-57. http://dx.doi.org/10.1016/j.jpowsour.2007.04.040

[23] Krongthong Kamonsuangkasem, Supaporn Therdthianwong, Apichai Therdthianwong, and Nirawat Thammajak, 'Remarkable Activity and Stability of Ni Catalyst Supported on Ceo2-Al2o3 Via Cealo3 Perovskite Towards Glycerol Steam Reforming for Hydrogen Production', *Applied Catalysis B: Environmental*, 218 (2017), 650-63. https://doi.org/10.1016/j.apcatb.2017.06.073

[24] Dongwook Kim, Derek R Vardon, Dheeptha Murali, Brajendra K Sharma, and Timothy J Strathmann, 'Valorization of Waste Lipids through Hydrothermal Catalytic

Conversion to Liquid Hydrocarbon Fuels with in Situ Hydrogen Production', *ACS Sustainable Chemistry & Engineering*, 4 (2016), 1775-84.

[25] Sebastian Kuntz, Oliver Berg, Christoph Sürgers, and Hilbert v Löhneysen, 'Signature of F-Electron Conductance in A-Ce Single-Atom Contacts', *Physical Review B*, 96 (2017), 085120.

[26] Di Li, Liang Zeng, Xinyu Li, Xiao Wang, Hongyan Ma, Suttichai Assabumrungrat, and Jinlong Gong, 'Ceria-Promoted Ni/Sba-15 Catalysts for Ethanol Steam Reforming with Enhanced Activity and Resistance to Deactivation', *Applied Catalysis B: Environmental*, 176-177 (2015), 532-41. https://doi.org/10.1016/j.apcatb.2015.04.020

[27] Lin Li, Dawei Tang, Yongchen Song, Bo Jiang, and Qian Zhang, 'Hydrogen Production from Ethanol Steam Reforming on Ni-Ce/Mmt Catalysts', *Energy*, 149 (2018), 937-43. https://doi.org/10.1016/j.energy.2018.02.116

[28] Yongjie Li, Rui Wang, Fengming Qi, and Chunming Wang, 'Preparation, Characterization and Microwave Absorption Properties of Electroless Ni–Co–P-Coated Sic Powder', *Applied Surface Science*, 254 (2008), 4708-15. http://dx.doi.org/10.1016/j.apsusc.2008.01.076

[29] Fang-hsin Lin, and Ruey-an Doong, 'Catalytic Nanoreactors of Au@ Fe3o4 Yolk–Shell Nanostructures with Various Au Sizes for Efficient Nitroarene Reduction', *The Journal of Physical Chemistry C*, 121 (2017), 7844-53.

[30] Sean S. Y. Lin, Do Heui Kim, and Su Y. Ha, 'Metallic Phases of Cobalt-Based Catalysts in Ethanol Steam Reforming: The Effect of Cerium Oxide', *Applied Catalysis A: General*, 355 (2009), 69-77. http://dx.doi.org/10.1016/j.apcata.2008.11.032

[31] Debora Marani, Christophe Gadea, Johan Hjelm, Per Hjalmarsson, Marie Wandel, and Ragnar Kiebach, 'Influence of Hydroxyl Content of Binders on Rheological Properties of Cerium–Gadolinium Oxide (Cgo) Screen Printing Inks', *Journal of the European Ceramic Society*, 35 (2015), 1495-504. http://dx.doi.org/10.1016/j.jeurceramsoc.2014.11.025

[32] B. Matas Güell, I. V. Babich, L. Lefferts, and K. Seshan, 'Steam Reforming of Phenol over Ni-Based Catalysts – a Comparative Study', *Applied Catalysis B: Environmental*, 106 (2011), 280-86. http://dx.doi.org/10.1016/j.apcatb.2011.05.012

[33] Yuanzhu Mi, Dingsheng Yuan, Yingliang Liu, Jingxian Zhang, and Yong Xiao, 'Synthesis of Hexagonal Close-Packed Nanocrystalline Nickel by a Thermal Reduction Process', *Materials Chemistry and Physics*, 89 (2005), 359-61. http://dx.doi.org/10.1016/j.matchemphys.2004.09.012

[34] M. Mokhtar, S. N. Basahel, and Y. O. Al-Angary, 'Nanosized Spinel Oxide Catalysts for Co-Oxidation Prepared Via Comnmgal Quaternary Hydrotalcite Route', *Journal of Alloys and Compounds*, 493 (2010), 376-84. https://doi.org/10.1016/j.jallcom.2009.12.106

[35] Bahador Nabgan, Tuan Amran Tuan Abdullah, Muhammad Tahir, Walid Nabgan, Yahya Gambo, Maryam Ibrahim, Ibrahim Saeh, and Kamal Moghadamian, 'Evaluation of Theoretical and Experimental Mass Transfer Limitation in Steam Reforming of Phenol-Pet Waste to Hydrogen Production over Ni/La-Promoted Al2o3 Catalyst', *Journal of Environmental Chemical Engineering*, 5 (2017), 2752-60. https://doi.org/10.1016/j.jece.2017.05.014

[36] Bahador Nabgan, Tuan Amran Tuan Abdullah, Muhammad Tahir, Walid Nabgan, Sugeng Triwahyono, Aishah Abdul Jalil, Yahya Gambo, Maryam Ibrahim, and Kamal Moghadamian, 'Pellet Size Dependent Steam Reforming of Polyethylene Terephthalate Waste for Hydrogen Production over Ni/La Promoted Al2o3 Catalyst', *International Journal of Hydrogen Energy*, 42 (2017), 21571-85. http://dx.doi.org/10.1016/j.ijhydene.2017.07.103

[37] Bahador Nabgan, Walid Nabgan, Tuan Amran Tuan Abdullah, Muhammad Tahir, Yahya Gambo, Maryam Ibrahim, and Wong Syie Luing, 'Parametric Study on the Steam Reforming of Phenol-Pet Solution to Hydrogen Production over Ni Promoted on Al2o3-La2o3 Catalyst', *Energy Conversion and Management*, 142 (2017), 127-42. http://dx.doi.org/10.1016/j.enconman.2017.03.046

[38] Bahador Nabgan, Muhammad Tahir, Tuan Amran Tuan Abdullah, Walid Nabgan, Yahya Gambo, Ramli Mat, and Ibrahim Saeh, 'Ni/Pd-Promoted Al2o3–La2o3 Catalyst for Hydrogen Production from Polyethylene Terephthalate Waste Via Steam Reforming', *International Journal of Hydrogen Energy*, 42 (2017), 10708–21. http://dx.doi.org/10.1016/j.ijhydene.2017.02.034

[39] Walid Nabgan, Tuan Amran Tuan Abdullah, Ramli Mat, Bahador Nabgan, Umi Aisah Asli, and Anwar Johari, 'Hydrogen Production from Phenol Steam Reforming over Ni-Co/Zro2 Catalyst: Effect of Catalyst Dilution', *Jurnal Teknologi*, 78 (2016), 77–82 http://dx.doi.org/10.11113/jt.v78.9569

[40] Walid Nabgan, Tuan Amran Tuan Abdullah, Ramli Mat, Bahador Nabgan, Aishah Abdul Jalil, Lutfi Firmansyah, and Sugeng Triwahyono, 'Production of Hydrogen Via Steam Reforming of Acetic Acid over Ni and Co Supported on La2o3 Catalyst', *International Journal of Hydrogen Energy*, 42 (2017), 8975-85. http://dx.doi.org/10.1016/j.ijhydene.2016.04.176

[41] Walid Nabgan, Ramli Mat, Tuan Amran Tuan Abdullah, Bahador Nabgan, Yahya Gambo, and Zaki Yamani Zakaria, 'Development of a Kinetic Model for Hydrogen Production from Phenol over Ni-Co/Zro2 Catalyst', *Journal of Environmental Chemical Engineering*, 4 (2016), 4444-52. http://dx.doi.org/10.1016/j.jece.2016.10.013

[42] Walid Nabgan, Tuan Amran Tuan Abdullah, Ramli Mat, Bahador Nabgan, Yahya Gambo, and Kamal Moghadamian, 'Acetic Acid-Phenol Steam Reforming for Hydrogen Production: Effect of Different Composition of La2o3-Al2o3 Support for Bimetallic Ni-Co Catalyst', *Journal of Environmental Chemical Engineering*, 4 (2016), 2765-73. http://dx.doi.org/10.1016/j.jece.2016.05.030

[43] Walid Nabgan, Tuan Amran Tuan Abdullah, Ramli Mat, Bahador Nabgan, Yahya Gambo, and Sugeng Triwahyono, 'Influence of Ni to Co Ratio Supported on Zro2 Catalysts in Phenol Steam Reforming for Hydrogen Production', *International Journal of Hydrogen Energy*, 41 (2016), 22922-31. http://dx.doi.org/10.1016/j.ijhydene.2016.10.055

[44] Walid Nabgan, Tuan Amran Tuan Abdullah, Ramli Mat, Bahador Nabgan, Sugeng Triwahyono, and Adnan Ripin, 'Hydrogen Production from Catalytic Steam Reforming of Phenol with Bimetallic Nickel-Cobalt Catalyst on Various Supports', *Applied Catalysis A: General*, 527 (2016), 161-70. http://dx.doi.org/10.1016/j.apcata.2016.08.033

[45] J. Staun Olsen, L. Gerward, U. Benedict, and J. P. Itié, 'The Crystal Structure and the Equation of State of Cerium Metal in the Pressure Range 0–46 Gpa', *Physica B+C*, 133 (1985), 129-37. https://doi.org/10.1016/0378-4363(85)90406-1

[46] Paula Osorio-Vargas, Cristian H. Campos, Rufino M. Navarro, José L. G. Fierro, and Patricio Reyes, 'Rh/Al2o3–La2o3 Catalysts Promoted with Ceo2 for Ethanol Steam Reforming Reaction', *Journal of Molecular Catalysis A: Chemical*, 407 (2015), 169-81. http://dx.doi.org/10.1016/j.molcata.2015.06.031

[47] Paula Osorio-Vargas, Nicolás A. Flores-González, Rufino M. Navarro, Jose L. G. Fierro, Cristian H. Campos, and Patricio Reyes, 'Improved Stability of Ni/Al2o3 Catalysts by Effect of Promoters (La2o3, Ceo2) for Ethanol Steam-Reforming Reaction', *Catalysis Today*, 259, Part 1 (2015), 27-38. http://dx.doi.org/10.1016/j.cattod.2015.04.037

[48] Qingqing Peng, Yongwen Tao, Huajuan Ling, Zhenyuan Wu, Zhanglei Zhu, Rongli Jiang, Yuemin Zhao, Yuelun Wang, Chen Ji, Xiaozhou Liao, Anthony Vassallo, and Jun Huang, 'Tuning Hydrogen and Carbon Nanotube Production from Phenol Steam Reforming on Ni/Fe-Based Nanocatalysts', *ACS Sustainable Chemistry & Engineering*, 5 (2017), 2098-108. 10.1021/acssuschemeng.6b01936

[49] K. Polychronopoulou, A. Bakandritsos, V. Tzitzios, J. L. G. Fierro, and A. M. Efstathiou, 'Absorption-Enhanced Reforming of Phenol by Steam over Supported Fe Catalysts', *Journal of Catalysis*, 241 (2006), 132-48. http://dx.doi.org/10.1016/j.jcat.2006.04.015

[50] K. Polychronopoulou, C. N. Costa, and A. M. Efstathiou, 'The Role of Oxygen and Hydroxyl Support Species on the Mechanism of H2 Production in the Steam Reforming of Phenol over Metal Oxide-Supported-Rh and -Fe Catalysts', *Catalysis Today*, 112 (2006), 89-93. http://dx.doi.org/10.1016/j.cattod.2005.11.037

[51] K. Polychronopoulou, J. L. G. Fierro, and A. M. Efstathiou, 'The Phenol Steam Reforming Reaction over Mgo-Based Supported Rh Catalysts', *Journal of Catalysis*, 228 (2004), 417-32. http://dx.doi.org/10.1016/j.jcat.2004.09.016

[52] N. Rahemi, M. Haghighi, A. A. Babaluo, M. F. Jafari, and P. Estifaee, 'Co2 Reforming of Ch4 over Ceo2-Doped Ni/Al2o3 Nanocatalyst Treated by Non-Thermal

Plasma', *Journal of Nanoscience and Nanotechnology*, 13 (2013), 4896-908. 10.1166/jnn.2013.7585

[53] Cyrille Rioche, Shrikant Kulkarni, Frederic C. Meunier, John P. Breen, and Robbie Burch, 'Steam Reforming of Model Compounds and Fast Pyrolysis Bio-Oil on Supported Noble Metal Catalysts', *Applied Catalysis B: Environmental*, 61 (2005), 130-39. http://dx.doi.org/10.1016/j.apcatb.2005.04.015

[54] Khaled Saeed Baamran, and Muhammad Tahir, 'Thermodynamic Investigation and Experimental Analysis on Phenol Steam Reforming Towards Enhanced H2 Production over Structured Ni/Zntio3 Nanocatalyst', *Energy Conversion and Management*, 180 (2019), 796-810. https://doi.org/10.1016/j.enconman.2018.10.099

[55] Sonam V. Sancheti, Chetana Saini, Rohini Ambati, and Parag R. Gogate, 'Synthesis of Ultrasound Assisted Nanostuctured Photocatalyst (Nio Supported over Ceo2) and Its Application for Photocatalytic as Well as Sonocatalytic Dye Degradation', *Catalysis Today*, 300 (2018), 50-57. https://doi.org/10.1016/j.cattod.2017.02.047

[56] D. P. Serrano, J. Aguado, J. M. Escola, J. M. Rodriguez, and A. Peral, 'Catalytic Properties in Polyolefin Cracking of Hierarchical Nanocrystalline Hzsm-5 Samples Prepared According to Different Strategies', *Journal of Catalysis*, 276 (2010), 152-60. https://doi.org/10.1016/j.jcat.2010.09.008

[57] Y. Z. Tang, M. Zhang, Z. Y. Wu, Z. G. Chen, C. B. Liu, Y. Lin, and F. Chen, 'Synthesis and Photocatalytic Activity of P-N Junction Ceo2/Co3o4 Photocatalyst for the Removal of Various Dyes from Wastewater', *Materials Research Express*, 5 (2018). 10.1088/2053-1591/aabdd8

[58] G. Vicente, J. Aguado, D. P. Serrano, and N. Sánchez, 'Hdpe Chemical Recycling Promoted by Phenol Solvent', *Journal of Analytical and Applied Pyrolysis*, 85 (2009), 366-71. https://doi.org/10.1016/j.jaap.2008.10.007

[59] Syieluing Wong, Norzita Ngadi, Tuan Amran Tuan Abdullah, and Ibrahim Mohammed Inuwa, 'Catalytic Cracking of Ldpe Dissolved in Benzene Using Nickel-Impregnated Zeolites', *Industrial & Engineering Chemistry Research*, 55 (2016), 2543-55. 10.1021/acs.iecr.5b04518

[60] Junke Xu, Wei Zhou, Zhaojing Li, Jihui Wang, and Jianxin Ma, 'Biogas Reforming for Hydrogen Production over Nickel and Cobalt Bimetallic Catalysts', *International Journal of Hydrogen Energy*, 34 (2009), 6646-54. http://dx.doi.org/10.1016/j.ijhydene.2009.06.038

[61] Eun-hyeok Yang, Na Young Kim, Young-su Noh, Sung Soo Lim, Jae-Sun Jung, Jae Suk Lee, Gi Hoon Hong, and Dong Ju Moon, 'Steam Co2 Reforming of Methane over La1−Xcexnio3 Perovskite Catalysts', *International Journal of Hydrogen Energy*, 40 (2015), 11831-39. http://dx.doi.org/10.1016/j.ijhydene.2015.06.021

[62] Yongxing Yang, Cristina Ochoa-Hernández, Víctor A. de la Peña O'Shea, Patricia Pizarro, Juan M. Coronado, and David P. Serrano, 'Effect of Metal–Support Interaction on the Selective Hydrodeoxygenation of Anisole to Aromatics over Ni-

Based Catalysts', *Applied Catalysis B: Environmental*, 145 (2014), 91-100. http://dx.doi.org/10.1016/j.apcatb.2013.03.038

[63] Tao Zhang, Weiwei Li, and Jean-Philippe Croué, 'Catalytic Ozonation of Oxalate with a Cerium Supported Palladium Oxide: An Efficient Degradation Not Relying on Hydroxyl Radical Oxidation', *Environmental Science & Technology*, 45 (2011), 9339-46. 10.1021/es202209j

[64] Xuesong Zhang, Hanwu Lei, Gayatri Yadavalli, Lei Zhu, Yi Wei, and Yupeng Liu, 'Gasoline-Range Hydrocarbons Produced from Microwave-Induced Pyrolysis of Low-Density Polyethylene over Zsm-5', *Fuel*, 144 (2015), 33-42. https://doi.org/10.1016/j.fuel.2014.12.013

[65] Zhanming Zhang, Yiran Wang, Kai Sun, Yuewen Shao, Lijun Zhang, Shu Zhang, Xiao Zhang, Qing Liu, Zhenhua Chen, and Xun Hu, 'Steam Reforming of Acetic Acid over Ni–Ba/Al2o3 Catalysts: Impacts of Barium Addition on Coking Behaviors and Formation of Reaction Intermediates', *Journal of Energy Chemistry*, 43 (2020), 208-19. https://doi.org/10.1016/j.jechem.2019.08.023

[66] Huan-Ping Zhou, Hao-Shuai Wu, Jie Shen, An-Xiang Yin, Ling-Dong Sun, and Chun-Hua Yan, 'Thermally Stable Pt/Ceo2 Hetero-Nanocomposites with High Catalytic Activity', *Journal of the American Chemical Society*, 132 (2010), 4998-99.